Composites Part B 242 (2022) 110076

Contents lists available at ScienceDirect

Composites Part B

journal homepage: www.elsevier.com/locate/compositesb

Upgrading sodium montmorillonite into a reactive internal curing agent for sustainable cement composites through non-ionic functionalization

Dayou Luo, Jianqiang Wei *

Department of Civil and Environmental Engineering, Francis College of Engineering, University of Massachusetts Lowell, Lowell, MA, 01854, United States

ARTICLE INFO

Keywords:
Sodium montmorillonite
Non-ionic functionalization
B. Physical properties
B. Chemical properties
Pozzolanic reactivity

ABSTRACT

The role of non-ionic functionalization in modifying the physical and chemical properties of clay minerals and their potential as internal curing agents in cement composites have been remaining unclear. This work elucidates comprehensive insights into the functionalization of sodium montmorillonites (sMTs) with two non-ionic surfactants, t-octyl phenoxy poly ethoxyethanol (TX100) and polyethylene glycol ether (PEG10), and their influences on sMT properties. The results indicate that both TX100 and PEG10 are effectively intercalated into sMT resulting in increased interlayer spacing and hygroscopic swelling behavior. With the presence of functionalization, the water uptake capacity, ion exchange capacity, and dispersion of the sMT in both water and simulated cement pore solution are improved. With raised Al and Si dissolution, a significant improvement in pozzolanic reactivity of sMT is observed. Insights reported here pave a path for leveraging non-ionic functionalized sMT as a potential internal curing agent for cement hydration and concrete performance enhancement.

1. Introduction

Montmorillonite (MT), commercially known as bentonite, is a perceivable 2:1 layered-like clay that consists of two silicon tetrahedral sheets and an aluminum octahedral sheet in-between, with metal cations, like Ca^{2+}, Na^{+}, and Mg^{2+} [1], embraced within the interlayer spaces. By leveraging its high silicate and aluminate contents, abundant resources, cost-effectiveness, high pozzolanic reactivity, and low carbon emission [2], MT has been extensively used as a supplementary cementitious material (SCM) in cement composite and concrete. By partially replacing cement with MT with proper dosage, mechanical properties, durability, and sustainability of concrete can be improved thereby extending the service life and decreasing the maintenance costs of the structures [3]. It has been recognized that MT presents both favorable and adverse effects on cement hydration and concrete properties. The cement hydration could be enhanced by the incorporation of MT, which is probably due to 1) "filler effects" from the fine particle size and high specific surface area, and 2) the desirable pozzolanic reaction [4]. Regarding the former mechanism, although the MT is less reactive than Portland cement, numerous nucleation sites for the precipitation of cement hydration products can be created by dispersing the small MT particles in the paste [5]. The latter suggests that additional calcium silicate hydrates (C–S–H) and calcium aluminate silicate hydrates (C-A-S-H) can be formed from the pozzolanic reaction between MT and calcium hydroxide (CH) produced from cement hydration [6]. Moreover, with the incorporation of MT, the permeability of concrete could be decreased, resulting in lower penetrations of external water and aggressive salts and hence increased resistance to a variety of deteriorations, such as corrosion [7], sulfate attack [8], and alkali-silica reaction (ASR) [9]. Consequently, both the microstructure and durability of the cement matrix could be improved with denser phases and more stable bonding frameworks [9]. Moreover, Chen et al. [10] reported that the static yield stress could be improved by adding MT into concrete, thereby exhibiting a better resistance to structural deformation over time. Researchers [10,11] have unveiled that the beneficial replacement level of MT on the mechanical properties (both flexural and compressive strength) is lower than 3% by weight, and the optimal results were reached at around 1%. Exceeding this benefit dosage, the mechanical properties of cement composites could be decreased by MT. On the other hand, a detrimental effect on workability with the increasing incorporation of MT was also reported. The high water absorption capacity and fine particle sizes [12], as well as the particle agglomeration caused by van der Waals force and electrostatic force between MT nanosheets in concrete mixing [13], are challenges for its broad application. Therefore, it is critical to address these challenges via a practical approach to enhance the positive role of MT in improving the

* Corresponding author.,
E-mail address: Jianqiang_Wei@uml.edu (J. Wei).

https://doi.org/10.1016/j.compositesb.2022.110076
Received 27 January 2022; Received in revised form 7 June 2022; Accepted 14 June 2022
Available online 18 June 2022

properties and sustainability of concrete.

Different from the conventional curing process of providing additional water for concrete externally via ponding, fogging, sealing, or covering with wet burlap, internal curing (IC) could pledge the entire three-dimensional microstructure of the hydrating cement paste accessible to the proper amount of water and free in autogenous shrinkage stress by introducing water reservoirs, such as pre-wetted lightweight aggregates, superabsorbent polymer, fly or bottom ashes [14–16]. With a more uniform distribution of additional water than the conventional external curing to fuel the hydration reactions, IC has become a promising method for producing concrete with increased performance as it could maximize cement hydration, minimize self-desiccation and improve the mechanical strength of concrete [17]. According to Power's model [18], only 0.23 g of water is theoretically required to fully hydrate 1 g of cement. However, based on the volumetric composition of the cement-based material, Jensen and Hansen [19] found that only when approximately 0.19 g of additional water per gram of cement is maintained as the capillary water unimpededly accessible for cement hydration, namely a water to cement (w/c) ratio of 0.42 (0.23 + 0.19), the cement hydration is possible to be fully completed. Therefore, the amount of water required in IC to compensate for the volume deformation of chemical shrinkage and obtain complete cement hydration could be calculated accordingly [19]. Although it was validated that the shrinkage of concretes could be eliminated via properly designed IC [14,20], some side effects were introduced and reported recently, such as compromises in compressive strength (slight) [21], flexural and tensile (drastic) [22], and modulus of elasticity [23]. According to Yang et al. [24], the effectiveness of IC depends on the amount of water introduced, the intrinsic properties of the IC agents, and the migration distance of the IC water. Noteworthy is the cation exchange capacity (CEC), swelling ability, water uptake, and the fine particle size implying MT potential as an IC agent, which can be leveraged to maximize the favorable aspects and eliminate the adverse effects of IC. However, the poor dispersion, low reactivity, uncontrolled water absorption and desorption, and unexploited retention of specific ions in the matrix of cement are still remained challenges.

A few methods, such as thermal, mechanical, and acid activations [25,26], have been studied to upgrade clay minerals into reactive SCMs. In a recent study by Cao et al. [27], thermal activation was found an effective approach to turn sandstone clay into a desirable SCM with high pozzolanic reactivity via dihydroxylation and alternation of Al and Si coordination. Mechanical ball milling also demonstrated a positive role to achieve partial dihydroxylation and activation of kaolin. As a facile chemical method, organic functionalization has been proven an effective approach to improve the properties of MT. Since the monovalent cations possess low charge densities and larger ionic radii than the divalent ones, lower hydration energy is needed [28]. The organic surfactants could be facilitated to enter the interlayer space of the sodium MT (sMT), as more water interleaving in the clay's interlayer space can be induced by the monovalent cations (Na^{+}) than the divalent ones (Ca^{2+} and Mg^{2+}). Therefore, extensive research has been dedicated to functionalizing pristine sMT with different surfactants, which has provided an opportunity to trigger superior clay properties for fabricating concrete with better mechanical properties, denser microstructures, decreased permeability, and improved durability. The functionalization can turn sMT into organo-sMT (OsMT) with enhanced hydrophobicity, thereby exhibiting negligible water adsorption and a reduced diffusion rate of aggressive chemical liquids in the modified cement mortar [29]. In line with the raw MT, it was found that the optimal incorporation dosage of OsMT for seeking both concrete strengths and durability is still less than 3% [29,30]. This could be explained by the decreasing dispersion of the clay particles in the cement matrix due to the increased hydrophobicity from the attachment of organic surfactants and less affinity with the inorganic dispersion [30]. The most commonly used surfactants are cationic, such as quaternary ammonium salts [30,31], which are known to be toxic and hazardous to the environment. To the best of our knowledge, concrete modification with functionalized OsMT based on less toxic and agglomerate non-ionic surfactants remains unexplored. It might be due to the hydrophilic character of the non-ionic surfactants, which can increase the water absorption and swelling behavior of sMT, thereby increasing the porosity and ion diffusion of concrete and decreasing the mechanical properties. In this study, a hypothesis that the increased water capacity may benefit cement modification via IC is leveraged to explore the potential of non-ionic OsMT as a desirable IC agent.

Leveraging this new perspective, the current study aims to investigate the influence of functionalization with two non-ionic surfactants with varying dosages on the physical and chemical properties of sMT clay particles. The potential of the functionalized OsMTs as novel IC agents in cement systems was also examined. Thermogravimetric analysis (TGA), X-ray diffraction (XRD), and attenuated total reflection-Fourier transforms infrared (ATR-FTIR) spectroscopy were performed to investigate the intercalation of surfactants into the clay particles, the change in clay's interlayer spacing, as well as the interaction between the surfactants and sMT. Dynamic vapor sorption (DVS), ATR-FTIR, swelling test, ultraviolet–visible (UV–vis) spectrophotometry, and inductively coupled plasma optical emission spectrometry (ICP-OES) were employed to characterize the behavior of OsMTs in terms of the moisture sorption isotherms, water up-take, water release, swelling, dispersion, and specific ion exchange. The pozzolanic reactivity was evaluated through integrated isothermal calorimetry and lime consumption test. Autogenous shrinkage and compressive strength tests were performed to evaluate the impact of OsMTs on concrete properties and the feasibility of using them as a new IC agent. A flowchart of the methods employed in this study is shown in Fig. 1.

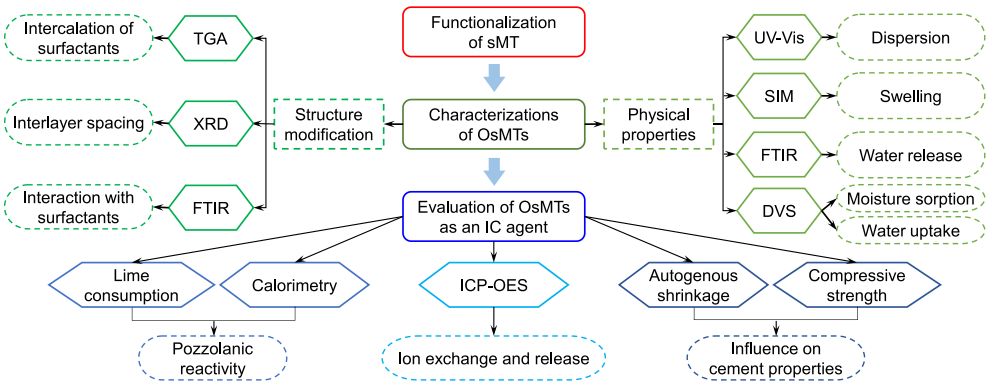

Fig. 1. Overview of tests and methods of this study.

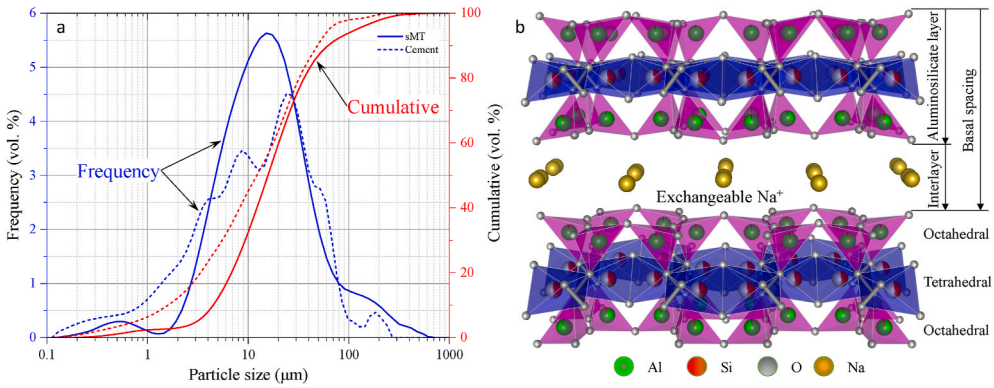

Fig. 2. (a) Particle size distributions of sMT and cement and (b) the layered structure of sMT.

2. Materials and methods

2.1. Materials

sMT purchased from Sigma-Aldrich with a relative density of 2.4 g/cm^3 and a molecular weight of 180.1 g/mol was used as the raw material for this study. Tpye I/II Portland cement produced by Quikrete was used in the autogenous shrinkage and compressive strength tests. The particle size distribution (PSD) of sMT and cement measured by laser diffraction is shown in Fig. 2a. The sMT exhibits a specific surface area and median particle size of 0.86 m^2/g and 7.9 μm, while the specific surface area and median particle size of the cement are 1.66 m^2/g and 12.2 μm, respectively. The chemical compositions of sMT and cement analyzed by X-ray fluorescence (XRF) and Bogue calculation are summarized in Table 1. It shows that the aluminosilicate (SiO_2 + Al_2O_3) content in the sMT is higher than 79 wt%. The schematic layered structure of sMT is shown in Fig. 2b, where an octahedral alumina sheet sandwiched between two tetrahedral silica sheets can be identified. The interlayer domain of sMT is occupied by Na^+, which balances the negative charge on sMT layers caused by the substitution of Al^{3+} by Mg^{2+} or Fe^{2+} in octahedral sheets [32]. The CEC of sMT is 116.48 meq/100 g, which was determined by Methylene blue test according to ASTM C 837 [33]. Extra pure CH with a purity of 98% was used for the lime consumption test, and deionized (DI) water was used for all investigations. Reagent grade CH (98%), sodium metasilicate (≥98%), sodium aluminate (99.9%), potassium hydroxide (97%), potassium sulfate (99.2%), and sodium hydroxide (97%) in deionized water (DI water, 18MΩ cm) were used for the preparation of simulated pore solution.

Two non-ionic surfactants, t-octyl phenoxy poly ethoxyethanol (TX100) and polyethylene glycol ether (PEG10), purchased from Sigma-Aldrich, were used for the functionalization. Both surfactants are chemically pure. The chemical structures of these two surfactants are presented in Fig. 3. TX100 and PEG10 share similar molecular structures, while the former contains one less carbon chain in length. The hydrophilic-lipophilic balance (HLB) values of TX100 and PEG10 are 13.5 and 13.0, respectively (a higher HLB value indicates higher hydrophilicity). The average molar mass of TX100 and PEG10 is 647 g/mol and 660 g/mol, respectively.

2.2. Functionalization of sMT

The functionalized OsMTs were prepared in an aqueous solution through the ion-exchange method [34]. The raw sMT particles were oven-dried at 105 °C for 24 h to remove free water. After cooling down in a sealed bottle at room temperature, the dry sMT particles were mixed with aqueous solutions with specific amounts of surfactants at a clay concentration of 100 g/L by stirring at 500 rpm for 30 min at 25 °C. The employed clay concentration and stirring speed have been proven effective protocols for intercalating surfactants into sMT as the layered clay structure of sMT can be collapsed at higher surfactant loadings resulting in the failure of functionalization. As summarized in Table 2, three dosages of the two surfactants equivalent to 0.2, 0.6, and 1.0 CEC were employed. The OsMTs were collected by centrifuging the suspension at 14000 rpm for 15 min to separate from aqueous solutions and washed twice with DI water. The obtained OsMTs were dried in an oven at 70 °C for 24 h, followed by grinding with a ball mill at 900 rpm for 2 h and sieving to obtain an average particle size smaller than 40 μm. As shown in Table 2, the OsMTs modified with different amounts of TX100 and PEG10 are expressed as "XY-sMT", where X is the equivalent loading of surfactants with respect to the CEC and Y is the surfactant name.

Table 1
Chemical compositions of sMT and cement (wt.%).

	CaO	SiO_2	Al_2O_3	SO_3	Fe_2O_3	MgO	SrO	K_2O	Na_2O	TiO_2	ZnO	ZrO_2	Cl	Rayleigh
sMT	0.949	62.0	17.2	0.199	6.51	7.35	0.0442	0.0717	5.03	0.224	0.0283	0.146	0.185	1.03
Cement	62.7	20.1	4.8	3.5	6.51	3.4	Na_2O + 0.658K_2O			C_3S	C_2S	C_3A	C_4AF	LS
							0.60			54	17	7	10	1.2

C_3S: tricalcium silicate; C_2S: dicalcium silicate; C_3A: tricalcium aluminate; C_4AF: tetra-calcium aluminoferrite; LS: limestone.

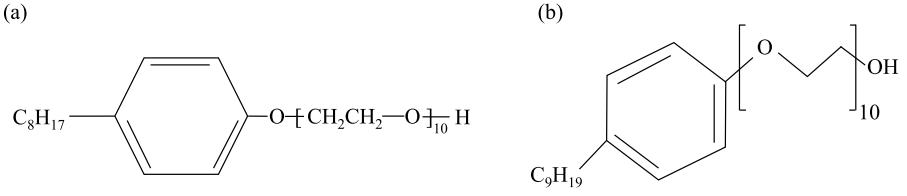

Fig. 3. Chemical structures of (a) TX-100; (b) PEG-10.

Table 2
A summary of preparation of organo-clays.

CEC	OsMTs	TX100/100 g sMT	OsMTs	PEG10/100 g sMT
0.2	0.2TX100-sMT	15.05 g	0.2PEG10-sMT	15.38 g
0.6	0.6TX100-sMT	45.15 g	0.6PEG10-sMT	46.13 g
1.0	1.0TX100-sMT	75.25 g	1.0PEG10-sMT	76.90 g

2.3. Characterizations

2.3.1. Thermogravimetric analysis

A thermogravimetric analyzer (TGA 4000 from PerkinElmer) was used to analyze the intercalation of the two non-ionic surfactants in sMT and the lime consumption capacity of the functionalized OsMTs. A heating rate of 15 °C/min from 30 °C to 800 °C was applied in an inert environment of N_2 purge gas at a 20 mL/min flow rate. Mass losses in different temperature ranges can be detected to quantify water evaporation, the amounts of surfactants, sMT decomposition, and consumption of CH. For the clay particles, 20–40 mg of the dried sMT and OsMTs were directly used for the TGA, while the sample preparations for the lime consumption test can be found in section 2.3.9 below.

2.3.2. X-ray diffraction analysis

The crystallinity and $d_{(001)}$ peak intensity of the sMT clay particles before and after functionalization were characterized by a Proto high accuracy powder X-ray diffractometer at 30 kV and 20 mA. The powder samples were scanned on a rotary support in stepwise mode with a step size of 0.02°(2θ) and a scanning time of 5 s per step in the range from 2.5 to 65° The basal spacing can be calculated based on the Bragg equation ($2d\sin\theta = n\lambda$), and the alteration of interlayer spacing of sMT in the presence of surfactants was quantified.

2.3.3. ATR-FTIR spectroscopy

The ATR-FTIR spectra of sMT and OsMTs were recorded with a Thermo Fisher Scientific Nicolet iS10 FTIR spectrometer. The spectra between 4000 and 400 cm^{-1} were acquired by the co-addition of 128 scans with a resolution of 4 cm^{-1} and a scanning time of 1.5 s per scan.

The raw sMT and selected OsMTs (0.2PEG10-sMT, 0.2TX100-sMT, 0.6PEG10-sMT, and 0.6TX100-sMT) were pre-saturated for 24 h, and then measured by ATR-FTIR within a spectra range between 4000 and 1500 cm^{-1}. The threshold relative humidity (RH) for cement hydration in concrete is about 80%, and the RH inside concrete after 28 days is in a range of 70%–85% varying with the w/c ratio and the depth from the concrete surface [35]. Therefore, after the 0-h test, the saturated samples were transferred to a sealed container with an equilibrium RH of 80% maintained by a saturated ammonium sulfate solution at room temperature, and the ATR-FTIR measurements in the spectra range of 4000 to 1500 cm^{-1} were conducted periodically for up to 72 h to explore the water release behavior of the pre-saturated functionalized clay particles.

2.3.4. Dynamic vapor sorption

DVS analysis was conducted under stepped RH between 0% and 95% at 25 °C to obtain a comprehensive understanding of moisture vapor absorption and desorption behavior of the sMT before and after functionalization. Around 20 mg of powder samples were used for testing. The wetting process started from an initial RH of 0, which was increased to 90% RH with a step size of 10%, followed by a final increase step to 95% RH. Subsequently, the desorption process was measured inversely under decreasing RH from 95% back to 0 with the same step size intervals. RH, temperature, and mass change were recorded at 1-min intervals. Equilibrium moisture content for each RH level was considered to be reached when the mass change of the samples became below 0.002%/min for 10 min.

The water uptake capacity (WUC) of the raw and functionalized sMTs to reach the saturated surface-dry (SSD) condition was determined via a modified drying rate method adapted from Ref. [36], which correlates the moisture status of clay particles with their drying rate when being exposed to constant ambient RH and temperature. DVS was used to monitor the moisture content of about 20 mg pre-saturated samples at a constant 40% RH and 40 °C. The data was recorded based on a 1-min interval and the equilibrium was assumed when the mass change is less than 0.001%/min for 10 min. The drying rate and drying acceleration were calculated based on the first and second derivatives of the mass development over time, respectively. The oven-dried weights of the samples were obtained after drying them at 105 °C until constant weights are reached, which were used to calculate the corresponding moisture contents (water to oven-dried clay mass ratio) for the drying acceleration and drying rate curves. At the beginning of the drying process, the extra free water on the surface of the clay particles evaporates at a high rate, which decreases gradually. Then, an inflection point appears indicating the complete removal of the surface water. After the inflection point, internal water starts to evaporate with a slower drying rate until an equilibrium state. Therefore, the inflection point in the drying rate curve (the peak of the drying acceleration curve reaches the peak) is considered to correspond to the clays' SSD condition, from where the WUC of sMTs to reach SSD conditions was determined accordingly.

2.3.5. Swelling tests

The influences of the surfactants on the swell potential of sMT were evaluated via a swell index method (SIM) per ASTM D 5890 [37]. 2.0 g of pre-dried pulverized samples 100% passing the No. 100 sieve (150 μm) with a minimum of 65% passing rate on the No. 200 sieve (75 μm) were used in this test. The clay samples were dusted over the entire surface of 90 mL of deionized water in a 100-mL graduated cylinder at increments of less than 0.1 g by tapping the particles out of a scoop for about 30s. Then, additional DI water was added to fill the cylinder to the 100-mL mark. The swelling volume of the samples defined by the interfaces between the sediment and the supernatant was measured after an elapsed time of 16 h and recorded in units of mL/2 g. All measurements were run in duplicate.

2.3.6. Synthesis of simulated pore solution and UV–vis spectroscopy

The simulated cement pore solutions were prepared by mixing reagent grade CH, sodium silicate, sodium aluminate, potassium hydroxide, potassium sulfate, and sodium hydroxide in DI water. The elemental concentrations of K, Na, Ca, Si, and Al are 493.63 mM, 44.93 mM, 2.44 mM, 0.15 mM, and 0.09 mM, respectively, which is comparable to the real pore solution from cement paste at 69 days according to Ref. [38]. The dispersion of the clay particles in the simulated pore solution is correlated to the characteristic absorbance peaks within the range of 210–300 nm and the slope after 300 nm up to 1000 nm. In this study, the UV–Vis spectroscopy was performed on a Cary 8454 spectrophotometer in a wavelength range of 210–1000 nm to evaluate the dispersion of sMT and OsMTs in a simulated cement pore solution with a pH value of 13.5. Right before the UV–Vis spectroscopy test, the mixed clay-pore solution samples were sealed in vials and ultrasonicated in an ultrasonic bath for 15 min.

2.3.7. ICP-OES

It is hypothesized that the increased interlayer spacing of sMT due to the intercalation of surfactants can provide a possibility of bearing more beneficial ions, such as Li^+, the incorporation of which has been proven a desirable and effective approach for ASR mitigation. However, it has been proven that Li^+ can result in accelerated early-age cement hydration and retarded hydration after 24 h with increased shrinkage [39]. Therefore, the absorption of Li^+ and its gradual release from the functionalized clay particles would play an essential role to guarantee both

chemophysical properties and durability of concrete. To evaluate the ion exchange and release behavior of specific cations of the functionalized sMT in the cement matrix, sMT and OsMT samples saturated with a $LiNO_3$ solution were investigated in the simulated cement pore solution. 5 g of each clay sample were mixed with 50 mL of 0.1 mol/L $LiNO_3$ solution for 30 min, followed by centrifugation at 10000 rpm for 10 min. After centrifugation, the clay particles were sedimented, and the remained Li^+ in the solutions collected from the suspensions was measured via inductively coupled-plasma optical emission spectrometry (ICP-OES), from where the amounts of Li^+ absorbed by the clay particles were determined. Then, the centrifuged clay samples were immersed in a 200 mL simulated cement pore solution stirring at 500 rpm and 40 °C for acceleration. 2.5 mL of the solutions were withdrawn at 2, 5, 10, 20, and 30 min. The collected solutions were then diluted by a factor of 250 with 2% nitric acid to stabilize the solutions, then filtered through 0.22 μm syringe filters. The concentrations of Li, Si, and Al were monitored by ICP-OES.

$$CH_1 = \left[\frac{W_{375} - W_{515}}{W_{515}} - f_s\right] \times \frac{M_{Ca(OH)_2}}{M_{H_2O}} = \left[\frac{W_{375} - W_{515}}{W_{515}}\right] \times 4.11 \times 100\% \quad (1)$$

$$CC = \left[\frac{W_{515} - W_{765}}{W_{765}}\right] \times \frac{M_{CaCO_3}}{M_{CO_2}} = \left[\frac{W_{515} - W_{765}}{W_{765}}\right] \times 2.27 \times 100\% \quad (2)$$

$$CH_2 = CC \times \frac{M_{CaCO_3}}{M_{Ca(OH)_2}} = CC \times 0.74 \quad (3)$$

where CH_1 and CC are the contents of CH and calcium carbonate, respectively. W_n is the mass at temperature n °C, M is the molar mass, and f_s is the mass fraction of the surfactants in OsMTs. Again, CH and CC thermal decomposition temperatures are determined based on tangent methods rather than fixed values.

By determining the CH contents, the consumption of CH by sMT/OsMTs was calculated by subtracting the retained CH from the initial mass ($m_{o,CH}$) and normalized by the mass of the clay samples.

$$CH\ consumption\ (g\ /\ 100g\ raw\ clays) = \left\{\left[m_{o,CH} - (CH_1 + CH_2) \times 39\right] \times \frac{100}{9}\right\} \Big/ (1 - f_s) \quad (4)$$

2.3.8. Isothermal calorimetry studies

It has been evidenced that isothermal calorimetry can be used to indirectly assess the pozzolanic reactivity of SCMs by measuring the heat released from the reaction between SCMs and CH. In the current study, the heat flow and release of the reactions between sMT/OsMT and CH up to 50 h at 25 °C were performed with an I-Cal 2000 HPC high precision isothermal calorimeter. All the blends were prepared by mixing sMT/OsMTs and CH at a ratio of 0.3 and a water-to-solid (w/s) ratio of 1.0. For each measurement, the raw materials, i.e., sMT/OsMT, CH, and mixing water, were sealed and conditioned in the calorimeter chambers at the target temperature of 25 °C for 24 h. About 50 g of blends were mixed by hand for 1 min at a temperature of 25 ± 2 °C. Then the samples were sealed in plastic containers and placed in the calorimeter chambers to record the evolutions of reaction heat.

2.3.9. Lime consumption test

As suggested by Suraneni and Weiss [40], a single test is not sufficient to predict the pozzolanic reactivity of SCMs. In addition to the calorimetry, the lime consumption (LC) test [41] was adopted as a direct method to determine the pozzolanic reactivity of sMT and OsMTs. For each test, 39 g of sMT/OsMT-CH blends (sMT/OsMT to CH ratio of 0.3) with a w/s ratio of 2.0 was cast in a high-density polyethylene bottle. About 20 mg of the blend powders were collected at 1, 7, and 28 days to determine the CH consumption by TGA with the same heating rate and temperature range as mentioned above. The contents of CH and $CaCO_3$ (CC) were determined based on the weight losses from 375 °C to 515 °C and from 515 °C to 765 °C, respectively. It is worth noting that the boundaries of thermal decompositions of CH and CC slightly vary for each sample, so the tangent method was employed to refine the corresponding temperature ranges. Although the intercalated surfactants do not participate in the pozzolanic reaction, the weight losses due to the decompositions of both TX100 and PEG10 are overlapped with that of CH. Therefore, as shown in Eq. (1), the contents of CH were determined by reducing the mass fraction of surfactants from the weight loss from 375 °C to 515 °C. CC is mainly due to the carbonation of CH during the process of sample preparation. Thus, the CH content was calculated by summing the CH from Eq. (1) and the CH_2 converted from CC in Eq. (2) and Eq. (3).

where, $m_{o,CH} = 30$ g, f_s is the mass fraction of surfactants in OsMTs.

2.3.10. Autogenous shrinkage

To evaluate the feasibility of using the functionalized OsMT in an IC agent for concrete, early-age (initial) autogenous shrinkage of the cement blends during the first 48 h was measured by a Schleibiger shrinkage cone, which is a precise laser-based system capable of touchless measuring shrinkage behavior immediately after the fresh cement paste is poured into the cone. In this study, the cement pastes were prepared by mixing the Portland cement, sMT or OsMTs, and water with a mechanical mixer. The clay particles (sMT or OsMTs) were pre-saturated for 24 h based on the determined WUC. 3 wt% cement was replaced with the pre-saturated clay particles, and the water-to-binder ratio was fixed at 0.35. It should be noted that the mass of the OsMTs was normalized by the mass fraction of sMT to ensure that each binary cement blends with sMT and OsMTs have the same amount of clay in the cement matrix. For easy comparison, an exact 300 g of paste for each group was tested. To eliminate water loss, the samples were sealed with paraffin oil right after installing the laser reflector.

2.3.11. Compressive strength

To evaluate the influence of OsMTs-based IC on the mechanical property of cement blends, the 28-day compressive strength of the cement mortars containing pre-saturated sMT and OsMTs was tested. As mentioned above, the optimal substitution level of MT in improving the mechanical strength of cement is 1%–3% by weight. In this study, 3 wt% substitutions of cement by saturated sMT and OsMTs were applied. Seven groups in total, namely the control group containing neat cement (PC), the group containing 3 wt% dry sMT (Dry sMT), the one containing 3 wt% pre-saturated sTM (Sat. sMT), and the groups containing 3 wt% pre-saturated OsMTs (0.2PEG10-sMT, 0.6PEG10-sMT, 0.2TX100-sMT, and 0.6TX100-sMT) were tested. The water-to-binder and cement-to-sand ratios for all the mortars were fixed at 0.4 and 1.0, respectively. After being cured in a saturated CH solution for 28 days, the compressive strength of the mortar mixtures was measured on 25 mm cubic mortar specimens with three repetitions for each group using a CONTROLS automatic concrete compression machine at a loading rate of 900 N/s according to ASTM C109 [42]. The peak load yielded by the samples was used for determining the compressive strength by averaging the three

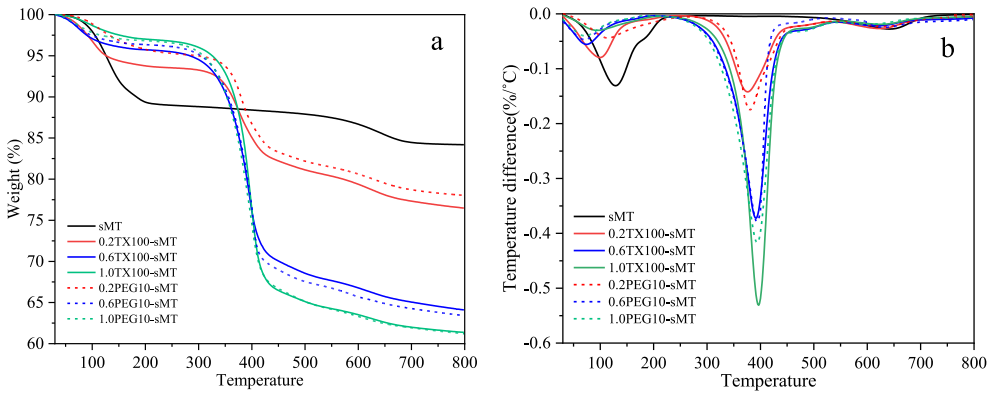

Fig. 4. (a) TGA and (b) DTG curves of sMT and OsMTs.

repetitions.

3. Results and discussion

3.1. Intercalation of surfactants into sMT

The amounts of the surfactants intercalated into sMT were determined from their thermal decompositions in TGA. The TGA and corresponding differential thermal analysis (DTG) curves of the raw sMT and OsMTs prepared with different concentrations of surfactants were given in Fig. 4a and b, respectively. The first peak at around 128 °C from the DTG curve of sMT was assigned to the evaporation of free interlayer water. This free water evaporation peak appears to shift to a lower temperature (69–100 °C) in the functionalized OsMTs. A lower DTG peak intensity with the increase of surfactant was observed, which might be due to the loss of free surface and interlayer water of sMT since the positions in the interlayer space of sMT are occupied by the surfactants. The slight weight loss corresponding to the DTG shoulder between 150 °C and 200 °C is caused by the loss of the water molecules bounded by exchangeable cations in the interlayer spaces. A decreased intensity of this bound water was also identified from the groups with higher dosages of surfactants, unveiling the exchanging process between cations and surfactants. The significant weight drop between 250 °C and 450 °C, which was observed from OsMTs only, is due to the decomposition of the intercalated surfactants. The corresponding DTG peaks' intensity increased with the dosage of surfactants indicating the more effective intercalation of the organic phases into sMT. A mass loss between 550 °C and 700 °C caused by dehydroxylation of sMT, which was decreased after the functionalization, was also detected.

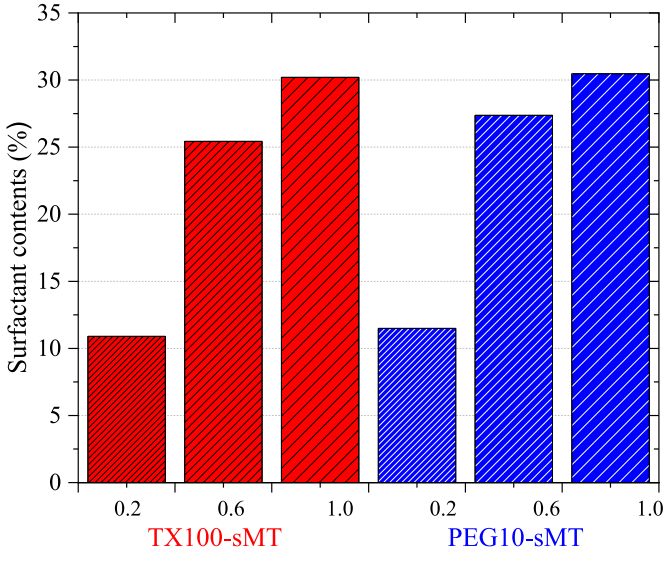

Fig. 5. Surfactant contents intercalated into sMT.

A modified interpretation method [43], which provides a relatively accurate determination of surfactants by considering the continuous slope of the TGA curve, was adapted to calculate the amounts of absorbed or intercalated surfactants in the OsMT. As shown in Fig. 5, PEG10 exhibited more effective intercalation into the sMT than TX100. After functionalization, the TX100-sMTs showed surfactant mass fractions of 10.9%, 25.4%, and 30.2% at TX100 loadings of 0.2 CEC, 0.6 CEC, and 1.0 CEC, respectively, while 11.5%, 27.4%, and 30.5% of PEG10-sMTs were occupied with PEG10 at the same loadings. This is consistent with the increase in the interlayer spacing (see section 3.2 below). The results obtained in the following sections are all normalized by the mass fraction of raw-sMT instead of the OsMTs.

3.2. Alterations of interlayer spacing

The XRD patterns of raw sMT and OsMTs functionalized by TX100 and PEG10 at varying loadings are shown in Fig. 6. The raw sMT exhibited a (001) reflection with a basal spacing of 1.52 nm (5.80° 2θ), which is in agreement with previous studies, e.g., 5.89° 2θ. In comparison, the corresponding values are 1.76 nm, 1.88 nm, and 3.27 nm for TX100-sMTs with the surfactant CEC loadings of 0.2, 0.6, and 1.0, respectively. The basal spacings of sMT were further enlarged in the presence of PEG10, which are 5.1%, 1.1%, and 0.9% higher than the TX100-sMTs at the same surfactant loadings. The basal spacing, calculated from the reflection peaks, represents a sum of the thickness of the sMT unit (tetrahedral + octahedral + tetrahedral, which is about 0.96 nm) and the interlayer spacing. Therefore, the interlayer spacing of sMT in this study is about 0.56 nm, which is increased to 0.8 nm, 0.92 nm, 2.31 nm in the presence of 0.2, 0.6, and 1.0 CEC TX100, and 0.89 nm, 0.94 nm, 2.34 nm by loading 0.2, 0.6 and 1.0 CEC PEG10, respectively. A new but small peak at around 16.50° 2θ was detected from the OsMTs, which increases with the loading of surfactants. The peek at 28.54° 2θ detected from the raw sMT shifted to the left with the surfactants and the d-spacing increased from 0.31 nm to 0.33 nm. The increased interlayer spacings evidence that both TX100 and PEG10 were intercalated into the interlayer space of sMT, which is consistent with the TGA results.

The surfactants can be intercalated into the layered structures of clays via different arrangement types, such as lateral monolayer, bilayer, pseudo trimolecular interlayer, and paraffin-bilayer. The low increase amplitude of the interlayer spacing indicates that both TX100 and PEG10 formed lateral monolayer arrangements inside sMT at 0.2 CEC and 0.6 CEC loadings. The substantial increase of the interlayer spacing of TX10-sMT and PEG10-sMT at 1.0 CEC loading implies the rearrangement of the surfactants from monolayer to a bilayer or even pseudo trimolecular structure in the interlayer of the clay mineral. In agreement with previous studies [34], such a phenomenon correlates the

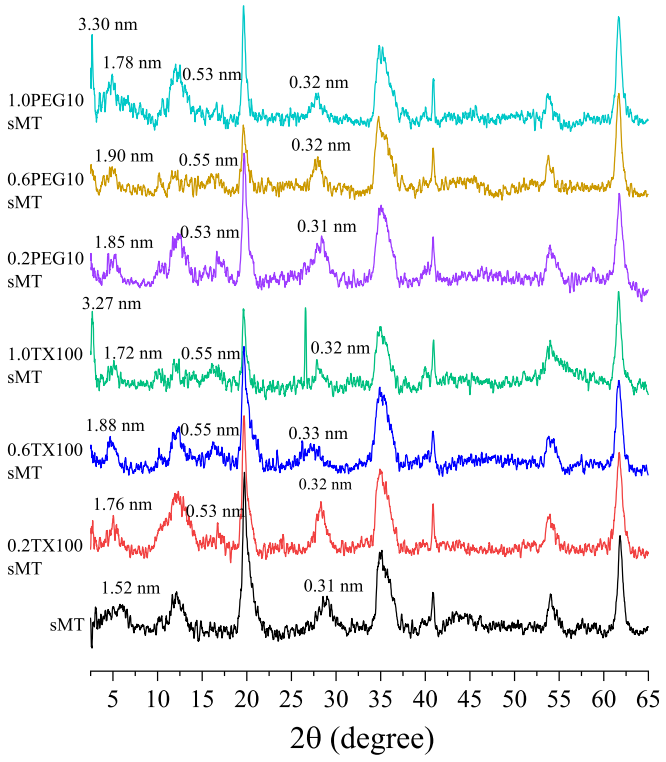

Fig. 6. XRD patterns of sMT and OsMTs.

arrangement type of the surfactants in the interlayer space of sMT clay particles with the surfactant loadings.

3.3. Interaction of sMT with surfactants

Fig. 7 shows the ATR-FTIR spectra of the pristine sMT and functionalized OsMTs from 4000 cm^{-1} to 400 cm^{-1}. The peak at around ~3615 cm^{-1} caused by the stretching vibration from the inner structural hydroxyl groups (Al–OH, Si–OH) shows decreased intensity after the functionalization with increasing loading of surfactants. Broadband centered at around 3405 cm^{-1} (symmetric and asymmetric stretching) and the peak at ~1632 cm^{-1} (bending vibration) allocated to the natural or absorbed water either on the surfaces or in the interlayer spaces of sMT exhibited lower intensity and a shift to the left in the presence of TX100 and PEG10. Moreover, the shoulder near 3225 cm^{-1}, due to the bending vibration of the cation hydration water in sMT, disappeared from the OsMTs. The absence of this spectral feature in OsMTs is due to the cation exchanged by surfactants and indicates fewer water molecules trapped in the interlayer of sMT/OsMT, which is consistent with the results from the TGA analysis. The peaks caused by the symmetric Si–O–Si bending mode (~972 cm^{-1}) in sMT shifted to the left in all OsMTs. This environmental change of SiO groups might be due to the interactions between tetrahedral silica sheets with the alkyl chains from surfactants. The asymmetric stretching mode of Si–O at 840 cm^{-1} increased with the intercalation of TX100 and PEG10. A partially overlapped peak at ~912 cm^{-1} attributed to the bending vibration of Al–Al–OH bonds [44], which was not impacted by the functionalization, was observed in both sMT and OsMTs. From the peaks at 510 cm^{-1} and 440 cm^{-1}, it was found that the bending absorptions of Si–O and Al–O bonds in the sMT's aluminosilicate structures [27,45] were not significantly altered by the functionalization.

The interactions between sMT and the two surfactants can be distinguished by two distinct spectral regions of 3025–2800 cm^{-1} and 1535-1175 cm^{-1} in OsMTs, which cannot be detected from sMT. The first spectral band here (3025-2800 cm^{-1}) is caused by the symmetric

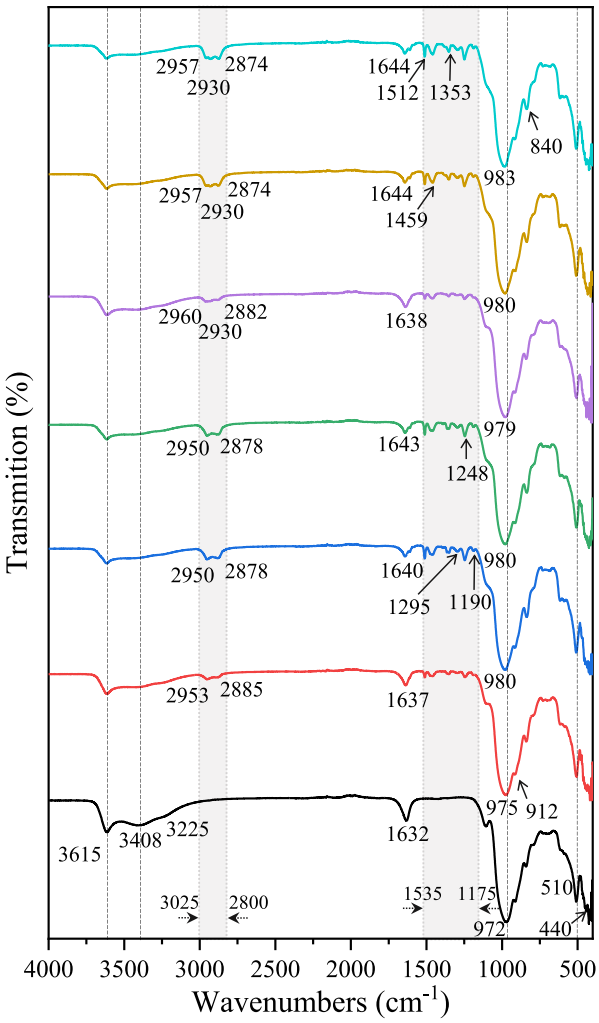

Fig. 7. FT-IR spectra of sMT and OsMTs with different surfactants' dosages.

and asymmetric stretching and bending vibrations of aliphatic chains ($–CH_2/–CH_3$) from the organic surfactants. The spectra from 1535 cm^{-1} to 1175 cm^{-1} consist of multiple distinct peaks. The two peaks at ~1248 cm^{-1} and 1190 cm^{-1} indicate the stretching vibrations of C–O–C from C_6H_5–O–C and $(CH_2CH_2O)_{10}$, respectively. The peak appearing at ~1353 cm^{-1} is assigned to the methylene deformation mode, and the one at ~1295 cm^{-1} is due to the C–O group attached with a methyl group or –OH bending group. The benzene ring skeleton in surfactants can be identified from the peaks at ~1512 cm^{-1} and ~1459 cm^{-1}, which indicates the symmetric stretching vibration of C═C from benzene rings. The intensity of these peaks increased with the dosages of TX100 and PEG10, while more intense and sharper peaks can be observed from PEG10-sMTs than TX100-sMTs at the same loading (dosage), providing an indication that PEG10 is more effective than TX100 in modifying sMT.

3.4. Dynamic moisture absorption and desorption

By varying the RH from 0% to 95%, the mass changes of sMT and OsMTs, normalized by the fraction of raw sMT, as a function of time for dynamic sorption kinetics of vapor and the corresponding isotherms were measured. From the moisture sorption profiles (Fig. 8a and c), it can be observed that, due to the intercalation of surfactants (both TX100 and PEG10), less time was taken by the OsMTs than the raw sMT to reach equilibrium in both the limbs of adsorption and desorption. It took about 50.5 h for sMT to complete the "adsorption-desorption" cycle,

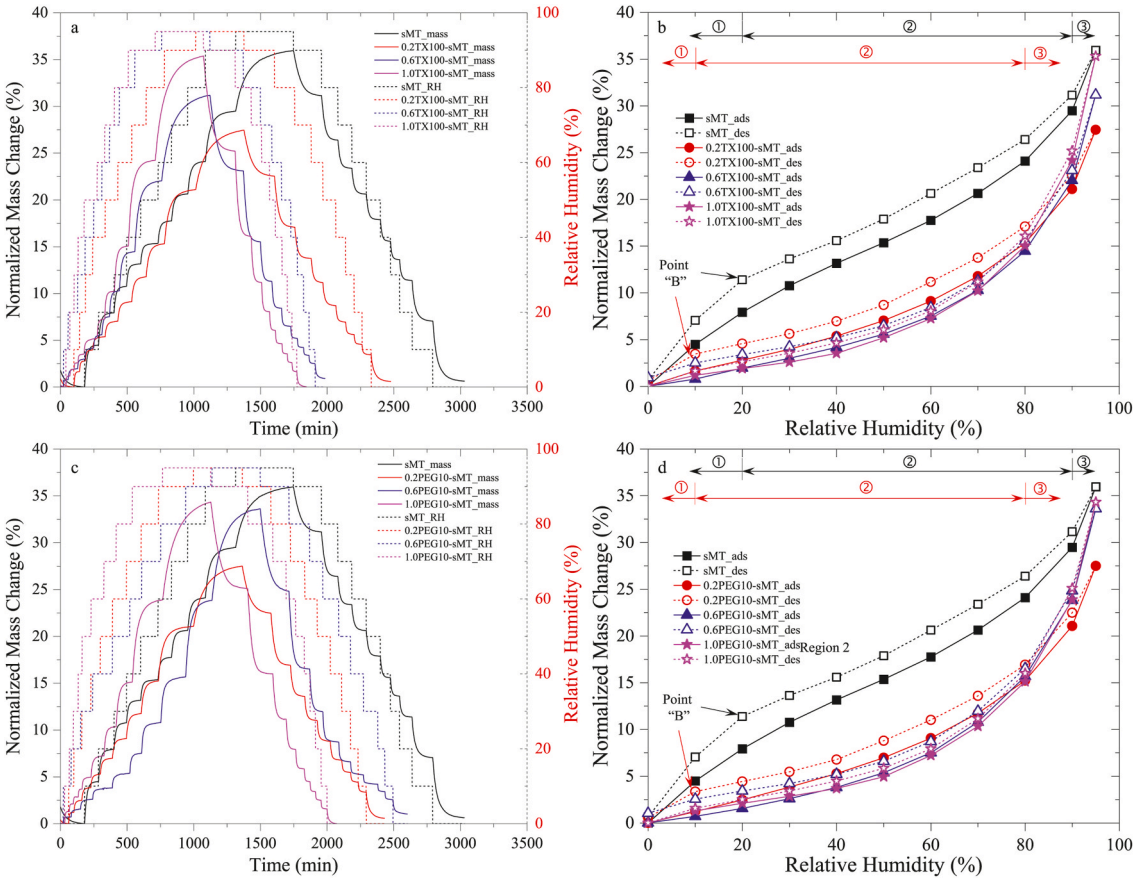

Fig. 8. Dynamic vapor sorption kinetics of (a) sMT and TX100-sMTs, (c) PEG10-sMTs; and isotherms of (b) sMT and TX100-sMTs, (d) PEG10-sMTs.

while 42 h, 33 h, and 30 h were taken by 0.2TX100-sMT, 0.6TX100-sMT, and 1.0TX100-sMT, respectively, showing a decrease in time needed with the dosage of TX100 intercalated. Being inconsistent with TX100-sMT, the OsMTs modified by PEG10 show the longest time for such one moisture sorption cycle at the intermediate dosage of 0.6CEC, followed by 0.2PEG10-sMT (40.5 h) and 1.0PEG10-sMT (34.5h). For the absorption stage, compared with the raw sMT, the length of the absorption stage was shortened by 21.3%, 36.1%, and 38.5%, respectively, in TX100-sMTs with increasing intercalation loadings. The same decreasing trend was also observed from the desorption session. 35.4% and 26.6% less time were taken by 1.0PEG10-sMT than sMT to finish the absorption and desorption processes, respectively.

The time needed at each RH period of sMT and OsMTs is summarized in Fig. 9. It can be seen that, for the absorption process, the time roughly increased with RH with a fluctuation between 20% and 50% RH. More significant concave curves were obtained during the desorption process, and the desorption between 40% and 30% for both sMT and OsMTs needs the minimum time. In the RH range between 0 and 30%, the raw sMT exhibits a longer equilibrium time than the OsMTs in both absorption and desorption stages. Interestingly, although the OsMTs exhibit a shorter time for a sorption cycle and decreased amount of moisture in comparison with the untreated sMT, a positive correlation between the moisture absorption capacity of the OsMTs and surfactant dosage was observed for both TX100 and PEG10. At their highest dosage (1.0 CEC), the final moisture equilibriums of TX100-sMT and PEG10-sMT at 95% RH are comparable to the raw sMT, but the time to reach

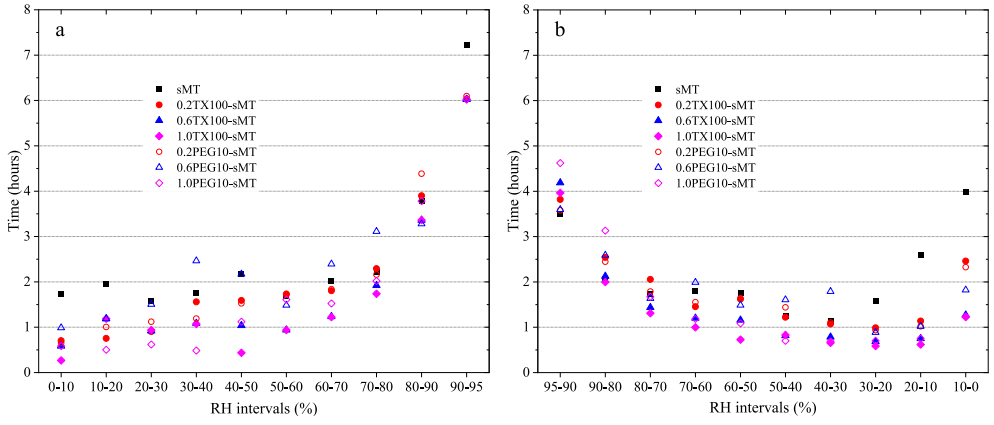

Fig. 9. The time needed for each RH equilibrium for sMT and OsMTs during (a) the adsorption and (b) the desorption process.

this equilibrium for both OsMTs is 16.6% shorter. The shortened time for both the absorption and desorption processes of the OsMTs discloses that the clay particles turn to be a weaker water vapor absorbent after functionalization.

According to Brunauer [46], there exist five types of sorption isotherms. Type I is the Langmuir adsorption isotherm commonly observed from microporous solids with a relatively small external surface. Type II is the S-shaped or sigmoid isotherm for non-porous or microporous adsorbents with unrestricted monolayer-multilayer adsorption. Type III represents the adsorption on the free particle surface. Type IV and V are related to the filling of pores and capillaries of mesoporous adsorbents and porous adsorbents with a weak adsorbent-adsorbate interaction, respectively. From Fig. 8b and d, the sorption isotherms of the raw sMT and OsMTs are in line with the type II pattern. This indicates that the moisture was adsorbed on the surface or the interlayer "walls" of the clay particles. Three segments can be identified from these sorption isotherms [47]: (1) a rapid increase in the moisture adsorption was observed before an inflection point (called the "B" point), which is 20% RH for sMT and 10% for OsMTs, indicating a monolayer adsorption period; (2) a moderate increase appears after the "B" point and up to 90% and 80% RH for sMT and OsMTs, respectively, triggered by the multilayer adsorption; (3) the sharp increase in moisture adsorption rate without a plateau in the end, which indicates the capillary condensation. It should be noted that, after the functionalization, the OsMTs yielded the monolayer adsorption in a lower RH with less adsorbed moisture with a higher dosage of surfactants, indicating a weaker water-clay interaction. On the other hand, the capillary condensation occurred earlier and was even more significant in the OsMTs than sMT, and it increased with the surfactant dosage, which resulted in a comparable final moisture uptake capacity at 1.0CEC. With the function treatments with TX100 and PEG10, the OsMTs show lower isotherms than the raw sMT, especially in the range of 10%–90% RH, suggesting that the OsMTs absorb less moisture in this particular RH range. This again suggests the increase in interlayer space by the intercalation of surfactants.

The significant hysteresis at high RHs from the isotherm curve of sMT evidences the existence of "ink-bottle" pores, which contain a narrow pore entry (neck) but a wide interior part (cavity) [48]. In this case, the intrusion of water molecules into the inner cavity occurs only if sufficient pressure is yielded in the narrow entries, that is, the cavity's filling happens after the neck. On the other hand, the evaporation during the desorption process follows the formation of a hemispherical meniscus in the narrow necks, acting as a pore blocker to obstruct the emptiness of the cavity. Thus, the moisture desorption within these "ink-bottle" pores might be induced by the narrow entry of the interlayer space in sMT, which is still filled or partially filled with moisture during the desorption process. However, the presence of hysteresis of clays at low RHs is still not well elucidated. The collapse or partial collapse of the interlayer structure during drying, which leads to retained moisture, might be one explanation. Another possible reason is the moisture retention by the crystalline cation hydration and the intermolecular forces, i.e., Coulomb attraction and London dispersion [49]. The hysteresis of the sMT from 10% to 90% RH is within the range from 1.7% to 3.5%, and it reaches the maximum at 20% RH, the minimum at 90% RH, and keeps in the level of around 2.5% in other RHs. On the contrary, the decreased hysteresis between the desorption and adsorption isotherms of the OsMTs, which further decreases with increasing surfactant dosage, illustrates the suppressed "ink-bottle" effect. With the increased opening entry or wider necks of the interlayer space of sMT by the intercalation of surfactants, the adsorbed moisture becomes easier to be desorbed resulting in the more negligible difference between the adsorption and desorption isotherms. Compared with that of sMT, the maximum hysteresis decreases to 1.8% and 1.7% for 0.2TX100-sMT and 0.6TX100-sMT at 10% RH, respectively, and it decreases further to 1.1% at 40% RH for 1.0TX100-sMT. While the similar decreasing trend with increasing RH was observed from PEG10-sMT (2.1% at 10% RH, 1.9% RH at 20%, 1.2% at 90% RH for the surfactants loading of 0.2, 0.6, and 1.0 CEC, respectively). Overall, the decreased hysteresis between adsorption and desorption over the whole RH range by the intercalation of surfactants into sMTs demonstrates the increasing interlayer space and an improved water release behavior, which is favorable to trigger IC in concrete.

3.5. Water uptake capacity

The WUC of the sMT and OsMTs was determined in terms of equilibrium moisture content under the SSD at 40% RH and 40 °C via DVS. Fig. 10a shows the weight drop of saturated samples during the drying process. It can be seen that the OsMTs need more time than the raw sMT to reach SSD mass equilibrium, which increases with surfactant dosage, indicating a stronger water absorption. Fig. 10b–h presents the drying rate and drying acceleration curves of sMT and OsMTs derived from their isotherms (Fig. 10a). From the drying acceleration curves, an inflection point corresponding to the moisture content of the SSD condition of the clay particles could be identified. Based on the assumption that the clay particles are in line with aggregate having four moisture states, i.e., absolutely dry, air dry, SSD, and wet conditions, the inflection point defines the boundary between the fully wet condition with extra water film on the surface and the SSD condition with water in interlayers and pores only. Therefore, by leveraging the different evaporation rates of surface water and inner water, the moisture content of the clay samples could be estimated from the inflection point.

By extracting the inflection points from Fig. 10, the WUC of sMT and OsMTs from dry condition to SSD was determined and presented in Fig. 11a, sMT exhibits a WUC of 13.9%. This value was increased significantly by the intercalation of non-ionic surfactants. With 0.2, 0.6, and 1.0 CEC TX100, the normalized WUCs of the OsMTs are 1.88, 3.41, and 3.73 folds of that of the raw sMT. For 0.2PEG10-sMTs, 0.6 PEG10-sMTs and 1.0PEG10-sMTs, 2.02, 3.00, and 3.01 folds of increase, respectively, were obtained. In addition to the hydrophilic feature of the surfactants, it is believed that the increase of WUC is due to the increased interlayer spacing of the OsMTs. As shown in Fig. 11b, a positive correlation between WUC and interlayer dimension is obtained. After the functionalization, the normalized WUC of sMTs was increased sharply from 13.9% to 26.2% and 47.4%, respectively, when the interlayer spacing increased from 0.56 nm (raw sMT) to 0.80 nm (0.2TX100-sMT) and 0.92 nm (0.6TX100-sMT). When the interlayer spacing of sMT was further increased from 0.92 nm to 2.31 nm, WUC was increased by 4.5%. The same trend was also observed from PEG10-modified OsMTs. With 0.2, 0.6 and 1.0 CEC PEG10, the WUC was increased to 28.1%, 41.8% and 41.9%, respectively. Interestingly, the slight increase in internal spacing within 1 nm results in significant improvement of WUC, while the more significant further expansion of internal spacing to 2.3 nm yields a less considerable increase in water uptake.

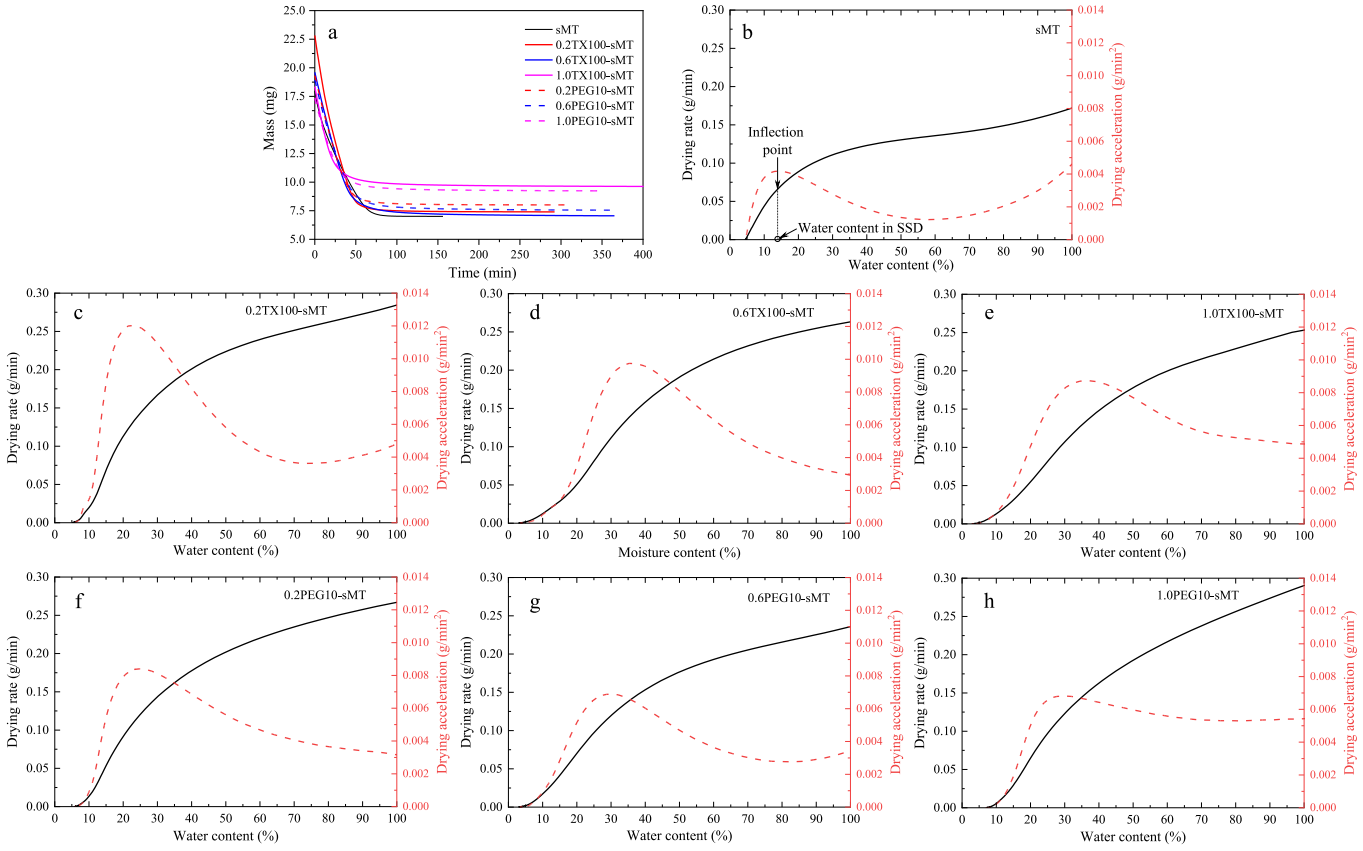

Fig. 10. (a) Mass change curves of saturated sMT and OsMTs at 40% RH and 40 °C, and (b–h) drying rate (black solid) and drying acceleration (red dash) curves of sMT and OsMTs. (For interpretation of the references to colour in this figure legend, the reader is referred to the Web version of this article.)

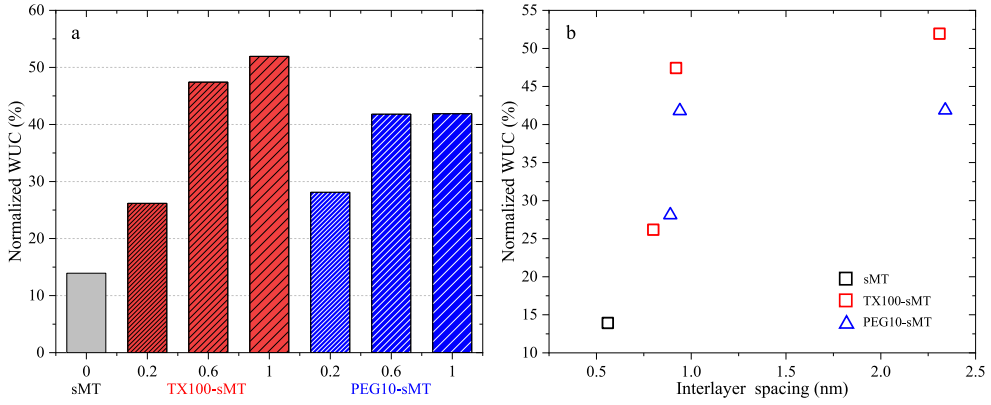

Fig. 11. (a) The normalized WUC of sMT and OsMTs and (b) the correlation between normalized WUC with the interlayer spacing determined from XRD.

3.6. Water release behavior

The O–H stretching between 3690 and 2400 cm^{-1} and bending at ~1640 cm^{-1} assigned to the water molecules under ATR-FTIR were leveraged to assess the water release behavior of the clay particles under 80% RH by monitoring the evolutions of peak intensity. Fig. 12 shows the ATR-FTIR spectra of the pre-saturated sMT and OsMTs conditioned under 80% RH in a wavenumber range of 4000–1500 cm^{-1}, from where a noticeable decrease in the peak intensity caused by water release over time is observed from all the clay particles. The raw sMT exhibited a significant water release after only 10 min. The intensity of the two peaks at 3690-2400 cm^{-1} and ~1640 cm^{-1} decreased by 4.7% and 1.7%, respectively. However, the water release rate slowed down significantly after about 3 h. After 72 h of exposure to 80% RH, the intensity of the two corresponding peaks decreased by 14.0% and 8.7%, respectively. By organically functionalizing sMT with surfactants, a more noticeable and sustained water release behavior was found over time (see Fig. 12b–e). For the 0.2PEG10-sMT and 0.2TX100-sMT, around 3.3% and 8.3% decreases in the intensity of the first peak (at 3690-2400 cm^{-1}) were detected after 30 min, respectively, and it decreased by 17.3% and 34.5% after 72 h. A more pronounced water release was observed from the OsMTs containing a higher dosage of surfactants (i.e., 0.6PEG10-sMT and 0.6TX100-sMT), the first peak of which decreased by 27.9% and 28.9%, respectively, after 72 h. The increased water release behavior from the OsMTs might be attributed to the enhanced WUC obtained after functionalization (see Section 3.5).

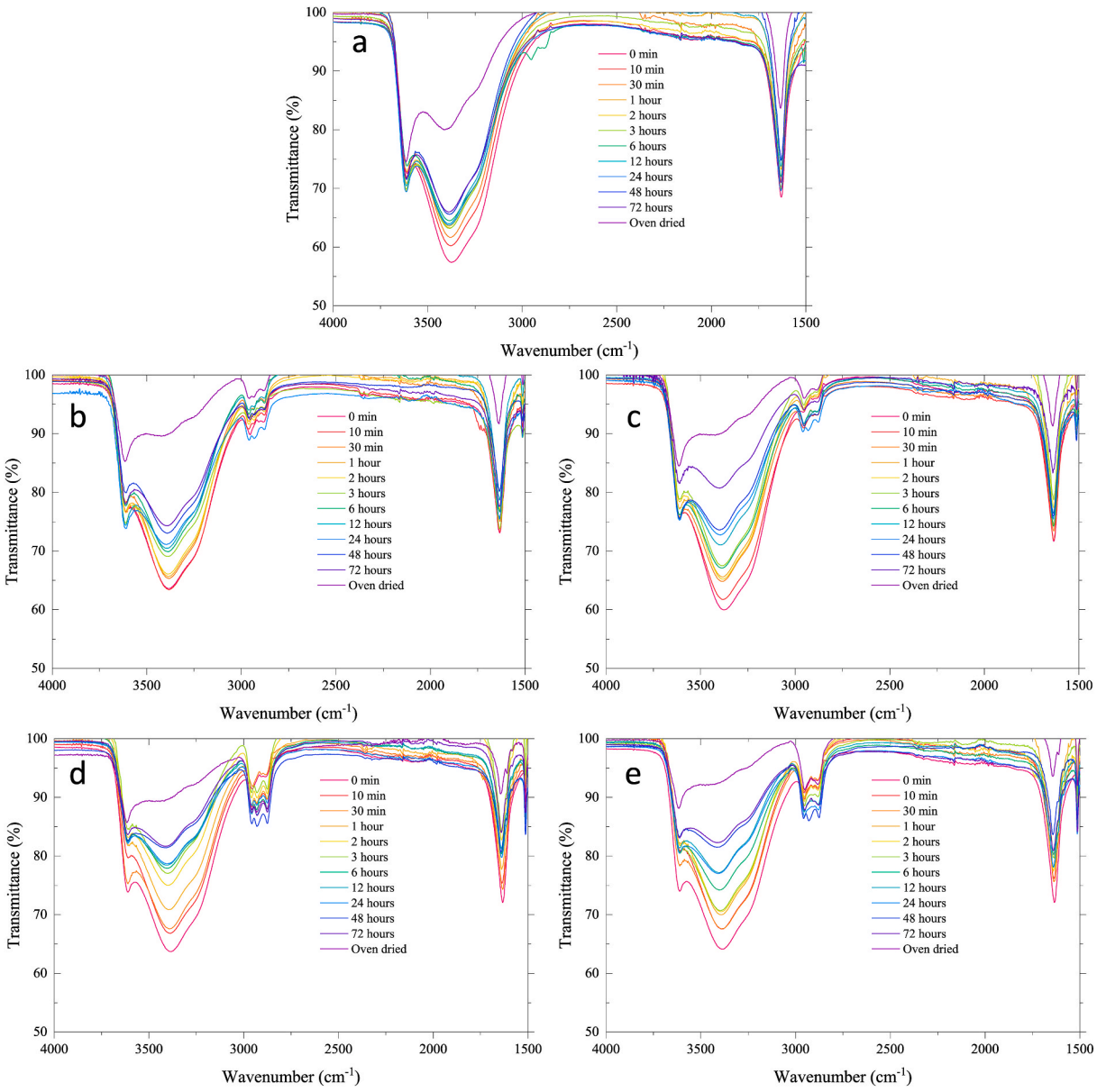

Fig. 12. ATR-FTIR spectra of the pre-saturated (a) sMT, (b) 0.2PEG10-sMT, (c) 0.2TX100-sMT, (d) 0.6PEG10-sMT, and (e) 0.6TX100-sMT exposed to 80% RH over time at 25 °C.

Moreover, the OsMTs presented a more sustained and gradual water release than the raw sMT, even at a relatively higher RH (i.e., 80%). Thus, it can be concluded that a more desirable water provision fueling cement hydration can be triggered by the OsMTs-based IC. It should be noted that the water-related peaks from all the samples are still higher than the oven-dried samples indicating that there is still some water remaining in the clay particles in the high RH environment. Compared with the untreated sMT, the amount of water in functionalized sMTs after 72 h showed lower differences from the oven-dried samples. This reveals that, after functionalization, sMT can not only load more water but also release the water more thoroughly, which further evidences the promising potential of the OsMT as an IC agent for concrete.

3.7. Swell behavior

Fig. 13a presents the swell indices of the sMT and OsMTs in DI water as a function of the CEC of surfactants. A positive correlation between swelling and dosage of surfactant is observed from both TX100 and PEG10-modified OsMTs with a neglectable difference. The raw sMT yielded a swell index of 12 mL/2 g. With intercalation of non-ionic surfactants, OsMTs showed 1.91 to 2.96 times higher swelling capacity, which is positively correlated to the dosage of surfactants. The two surfactants at the three dosages showed comparable efficiency in improving sMT's swelling capacity (the swell index of 0.2, 0.6, 1.0 TX100-sMT and 0.2, 0.6, 1.0 PEG10-sMT is approximately 23, 32, 35 and 23, 32.5, 35.5 mL/2 g, respectively). The swelling of MTs includes two phases: hydration swelling and osmotic swelling [50]. The hydration swelling (also known as crystalline swelling) occurs due to the hydration of both clay surfaces and exchangeable cations. In this stage, MTs can absorb up to four monolayers of water into the interlayer space. A greater interlayer swelling of MTs with monovalent cations (such as Na^{+}) could result from the osmotic phase, which can be commonly explained by the Gouy-Chapman diffuse double layer theory [51]. For the OsMTs, the increased interlayer space (see XRD analysis) and enlarged opening entry (see DVS analysis) make the access of external water into their internal spaces easier, which might be one reason for the improved swelling indices. Another possible reason is the presence of OH-groups of the intercalated surfactants, which can enhance the

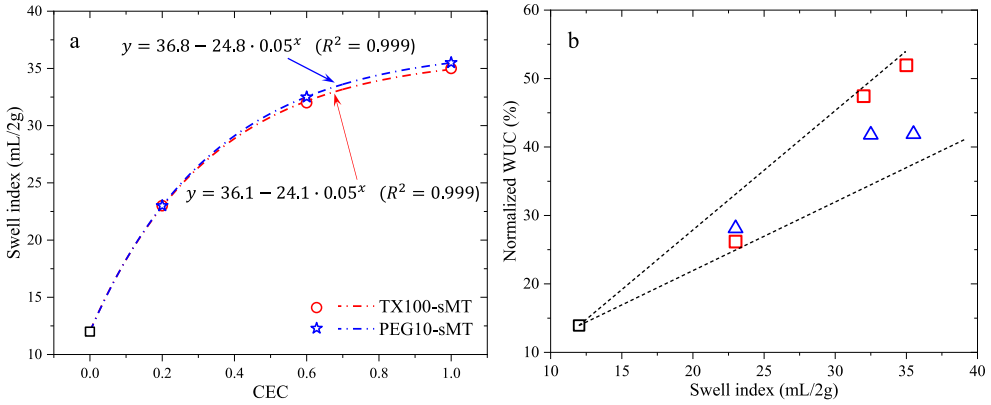

Fig. 13. (a) The correlation between the swelling index of sMT and OsMTs and dosage of surfactants, (b) the correlation between normalized WUC and swelling index.

hydrophilicity of the clay particles, thereby increasing the swelling potential. A positive correlation between the swelling index and normalized WUC of sMT and OsMT was elucidated in Fig. 13b. It is somewhat predictable as the normalized WUC increases with the interlayer space of OsMTs by the intercalation of surfactants, which provides more space for water ingress to result in a more pronounced swelling potential.

There might be favorable effects from the improved swelling behavior when using sMT as an IC agent or mineral admixture to partially replace cement in concrete. It was reported that cement hydration would not be significantly improved even enough water was introduced by IC in the cementitious system with a w/c ratio of 0.36 due to the low space availability for the precipitation of hydration products [19]. However, the increased reversible swelling behavior of OsMTs in this study makes it an ideal agent for IC, as it could contribute more space for the diffusion of cement hydration products in the hydrated concrete system. In terms of ASR mitigation, the improved swelling of sMT will provide additional tunable space for deposition of ASR gels, reduction of internal stress, healing of internal micro-cracks, and the creation of short-range connected pore networks to facilitate the directional transport of mitigating ions. However, an excessive expansion potential of sMT may cause detrimental expansion of the concrete structures after absorbing water. Thus, the swelling capacity of sMT and incorporation dosage should be well controlled to enhance the performance of concrete without side effects.

3.8. Dispersion in water and concrete pore solutions

The most critical challenge in using ultra-fine clay particles as SCMs is the poor dispersion in the matrix of cement. It's known that the net negative charge is the primary factor in clay dispersion, and the cations in the aquatic environment are the main driving force for flocculation. With a relative flocculating power of 43.0, calcium (Ca^{2+}) is defined as a stronger flocculator than sodium (Na^{+}) [52]. As a result, sMT exhibits lower dispersion and higher aggregation and flocculation in the high alkaline simulated pore solutions than DI water resulting in the decreased workability of the cementitious systems. According to Beer's law [53], the optical absorbance of the suspension in solution represents the concentration of the substance, as the absorbance is linearly correlated to the concentration of absorbing species. Based on this, to evaluate the influence of functionalization on the dispersion behavior of sMT particles at the initial and ongoing stages of mixing, UV–Vis analyses of sMT and OsMTs in both DI water and simulated pore solution within the 210–1000 nm wavelength range were performed. As can be seen from the diffuse reflectance spectra in Fig. 14a and b, the characteristic absorbance peaks at 223 nm and 274 nm for MT particles and organic molecules from surfactants could be readily identified from OsMTs. However, the former peak disappeared from the raw sMT clay particles dispersed in DI water, which might be due to its extremely poor dispersion. The higher absorbance, as well as the linear range at higher wavelengths, indicate better dispersion of the OsMTs in both DI water and simulated pore solution. It should be noted that the TX100-sMTs show a higher dispersion than the PEG10-sMTs in both DI water and simulated pore solution under the same surfactant loadings. In DI water, 0.2TX100-sMT shows the highest dispersion, while it decreased with the contents of TX100 intercalated into sMT. The dispersion of 0.6PEG10-sMT is higher than 0.2PEG10-sMT, but a decreased dispersion was observed at a higher dosage (1.0 CEC). In a simulated pore solution, the dispersion increases when the surfactants' loading is under 0.6CEC

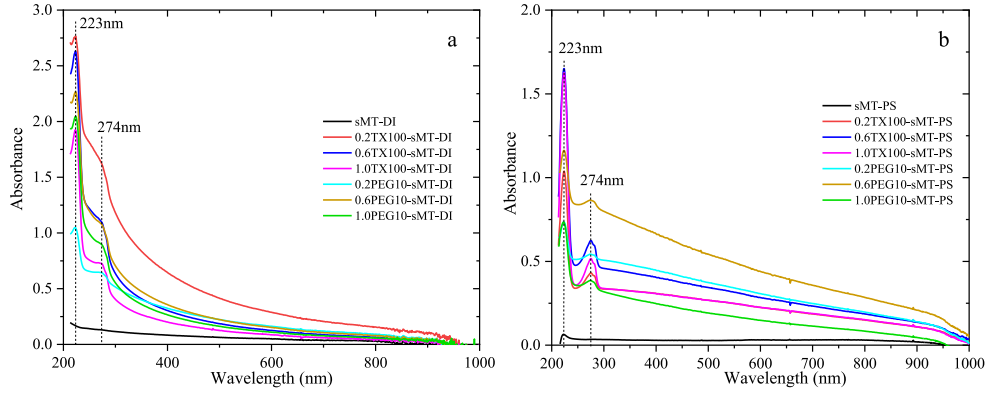

Fig. 14. UV–Vis spectrum of sMT and OsMTs in (a) DI water with a concentration of 0.2 mg/mL and (b) in simulated pore solution with a concentration of 1.0 mg/mL.

but then decreases when the surfactant loading is higher (1.0CEC), suggesting the agglomeration might occur again as the unit mass and particle size of OsMT increases with the loading of surfactants.

3.9. Ion release and exchange behavior

The absorption of Li^+ by the sMT and OsMTs after 30 min stirring in 0.1 mM $LiNO_3$ solution was monitored and presented in Fig. 15a. The raw sMT without functionalization exhibits a Li^+ absorption capacity of 58.2 mmol/100 g. In the presence of TX100 and PEG10, significant improvements of Li^+ absorption was observed, which increases with the surfactant dosages (the increments are 50.3%, 95.3%, and 120.0% for 0.2, 0.6, and 1.0 TX100, and 55.3%, 88.9%, and 106.5% for 0.2, 0.6, and 1.0 PEG10-sMT, respectively). The increased interlayer space of sMTs due to the intercalation of surfactants makes the clay capable of bearing more ions. In addition to the Li^+ bearing capacity, an effective release of Li^+ from the clay particles is also crucial to better mitigate concrete deteriorations like ASR. Towards this end, the Li^+ release behavior of sMT and OsMTs for up to 30 min in the simulated pore solution was monitored. As shown in Fig. 15b, the raw sMT released 52.9 mmol/100 g Li^+ after 2 min in the simulated pore solution, followed by an oscillation within the range of 52.88–55.90 mmol/100 g during the entire testing period. After 30 min of dissolution, around 93.4% of the Li^+ absorbed by the sMT can be released. After functionalization, a more effective Li^+ release rate, which also increases with surfactant dosage, was obtained from the OsMTs. After 30 min, and the amounts of Li^+ released by 1.0 TX100-sMTs and 1.0 PEG10-sMTs are 113.53% and 110.13%, respectively. The improvements in both Li absorption and release behavior indicate that, at the same substitution level, the functionalized OsMT can bear additional Li^+ into the cement mixture and subsequently release it. This enhanced feature is favorable to making sMT a multi-functional IC agent for modifying cement hydration and mitigating ASR.

Since sMT possesses a high pozzolanic reactivity due to its rich Al and Si components. The influence of non-surfactant functionalization on the dissolution of sMT in terms of Al and Si release has also been monitored in simulated pore solution. As shown in Fig. 16a and b, the release of both Al and Si exhibit quick equilibrium. The raw sMT shows Al and Si release in a range of 5.1–5.9 mmol/100 g and 5.0–7.6 mmol/100 g, respectively, and both increase during the first 10 h and then gradually decrease. Enhanced dissolution of sMT in cement pore solution was observed after functionalization. A faster dissolution of aluminate than silicate was observed from the functionalized OsMTs. Four groups (0.2TX100-sMT, 1.0TX100-sMT, 0.2PEG10-sMT, and 1.0PEG10-sMT) show sustained increase of Si release with time. It is worth mentioning that 0.2PEG10-sMT released the highest content of Al and Si into the simulated pore solution after 30 min of dissolution, which are 3.6 and 3.4 times over the raw-sMT, respectively. Both 0.6TX100-sMT and 0.6PEG10-sMT show the lowest Al and Si release among the OsMTs. By further increasing the dosages of the two surfactants, the release of both Al and Si increases again. The dissolutions of aluminate and silicate are the prerequisites of pozzolanic reactivity of clay minerals and directly determine the reaction kinetics. Therefore, the intercalations of the two non-ionic surfactants not only regulate the physical structure and properties of sMT (interlayer space, moisture sorption, water uptake, swelling, and dispersion behavior) but also enhance its chemical reactivity. To verify the hypothesis, the pozzolanic reactivity of sMT with and without the functionalization was studied.

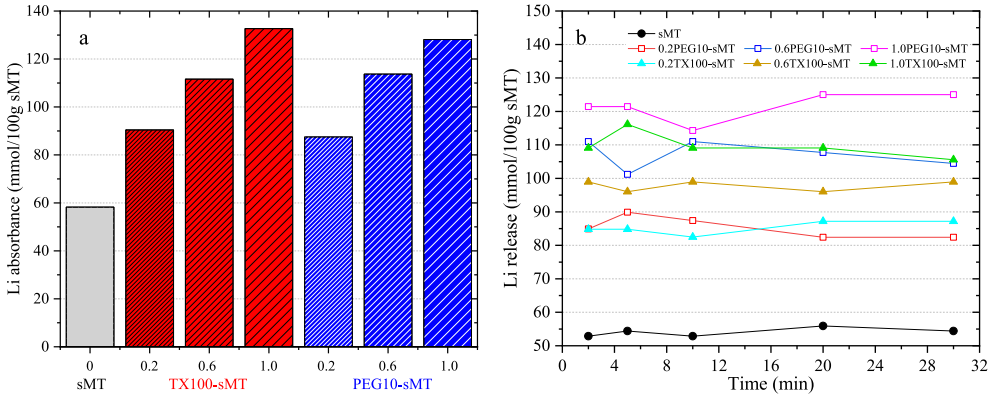

Fig. 15. Li (a) absorbance and (b) release behavior of sMT and OsMTs.

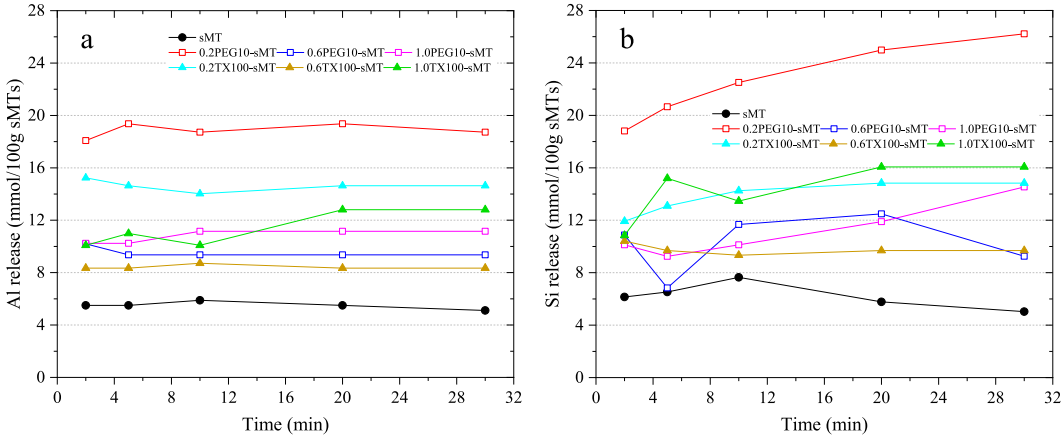

Fig. 16. (a) Al and (b) Si release behavior of sMT and OsMTs.

3.10. Pozzolanic reactivity

Pozzolans like sMT present a predominant pozzolanic reactivity as they are rich in amorphous silicate and aluminate, which can react with CH to form additional C–S–H [54]. Thus, a widely used indicator of pozzolanic reactivity is the consumption of lime, which can be categorized as a direct evaluation. Several methods, including the Chapelle method [55] and Frattini method [56], have been proposed to evaluate the pozzolanic reactivity of SCMs. The former measures the consumption of CH in a solid system, and the latter determines the concentrations of dissolved Ca^{2+} and OH^{-} in a solution. Moreover, indirect test methods commonly indicate the extent of pozzolanic reactivity of the SCMs by measuring the physical properties of the sample, such as strength activity index, electrical conductivity, and isothermal conduction calorimetry. Here, one indirect, isothermal conduction calorimetry, and one direct method, lime consumption test, were employed to assess the pozzolanic reactivity of the sMT before and after functionalization.

3.10.1. Calorimetry studies

The heat flow patterns and cumulative heat release of the reactions between CH and sMT/OsMTs at 25 °C normalized by the mass fraction of raw sMT are given in Fig. 17a and b, respectively. From Fig. 17a, the peak of heat flow was reached suddenly after blending CH and clay particles with water in all pastes. After about 0.05 h, the heat flow subsided gradually. It is seen that the amplitude of the peak and attenuation period of the normalized heat flow were dependent on the surfactants and their loadings. Compared with the raw sMT, the peaks of heat flow are higher with the intercalation of both TX100 and PEG10. For PEG10-sMT, 0.2PEG10-sMT presented the highest peak of heat flow among all the samples, which is in good agreement with the dissolutions of aluminate and silicate (see Fig. 16). 0.6PEG10-sMT exhibited less reaction heat and a further increased dosage to 1.0CEC resulted in enhanced reaction heat. Similar trends and differences are also identifiable in the normalized heat release curves (see Fig. 17b). After 50 h of reaction, 0.2PEG10-sMT, 0.6PEG10-sMT and 1.0PEG10-sMT released 40.3%, 30.2% and 35.9% more reaction heat than the raw sMT. For the OsMTs functionalized with TX100, different from PEG10-sMTs, the amplitude of the heat flow peak, length of attenuation period, and accumulative heat release are all positively correlated to the amount of intercalated surfactant. At all three dosages, TX100-sMTs released less reaction heat than PEG10-sMTs. The raised rection heat provides an indirect indication of the enhanced pozzolanic reaction between CH and sMT after being functionalized by the two surfactants.

3.10.2. Lime consumption test

The binary sMT-CH and OsMT-CH blends were thermogravimetrically analyzed at 1, 7, and 28 days. TGA and DTG curves are recorded in Fig. 18. From the DTG curves, three peaks could be identified from 30 °C to 200 °C. The first weight loss in the temperature range up to ~130 °C due to the elimination of physically bounded water. The second and third slight decompositions between 130 °C and 200 °C are mainly caused by the dehydration of the pozzolanic reaction products (C–S–H and C-A-S-H) produced by the lime and sMT/OsMTs [57]. Similar to metakaolin-CH systems [58], hydrogarnet (C_3ASH_6) decomposition has also been detected during the mass drop between 300 °C and 400 °C. The prominent weight between 400 °C and 500 °C (and the corresponding sharp DTG peak) is induced by the dehydration of CH [59]. The weight at around 740 °C due to the decomposition of calcium carbonate [60] was also observed indicating the occurrence of slight carbonation of CH during the sample preparation and test. By comparing the DTG curves for different ages, the peaks due to the decomposition of CH decreased gradually with time, while the weight losses caused by the decompositions of C–S–H and C-A-S-H increased over time. From the OsMT-CH blends, 0.2PEG10-sMT-CH shows the highest weight drops in the temperature intervals related to the decomposition of both C–S–H and C-A-S-H, indicating the highest pozzolanic reactivity.

By taking the carbonation of CH into account, the lime consumption capacity of sMt and OsMTs at different ages was calculated from the TGA curves by subtracting the remaining CH (including the CH converted from the carbonation) from the initial CH input. The normalized lime consumption by the mass fraction of sMT is given in Fig. 19a. The raw sMT showed a lime consumption capacity of 51.7, 58.5, and 68.2 g/100 g sMT at 1, 7, and 28 days, respectively. After functionalization, the lime consumption was remarkably increased, showing a positive correlation with the dosage of surfactants for all the testing ages. For TX100-sMTs, the increasing trend is consistent with the results from the calorimetry study above (see Fig. 17). At 28 days, 68.2%, 203.9% and 265.5% more CH was consumed by 0.2TX100-sMT, 0.6TX100-sMT and 1.0TX100-sMT, respectively. Compared with TX100, PEG10 exhibits a more effective enhancement of lime consumption capacity of sMT at 0.2CEC and 0.6CEC. At 1.0CEC, the two non-ionic surfactants are comparable. Fig. 19b illustrates the positive correlation between the equilibrium concentration of Al + Si from sMT and OsMTs in pore solution after 30 min of dissolution and the normalized CH consumption from the sMT/OsMT + CH blends after 28 days. It can be found that 68.2 g CH was consumed per 100 g sMT when 10.13 mmol of Al + Si was dissolved in the simulated pore solution. The functionalization with the two surfactants enhanced the dissolution of Al and Si from OsMT to pore solution, thereby consuming more CH than the raw sMT. The two surfactants

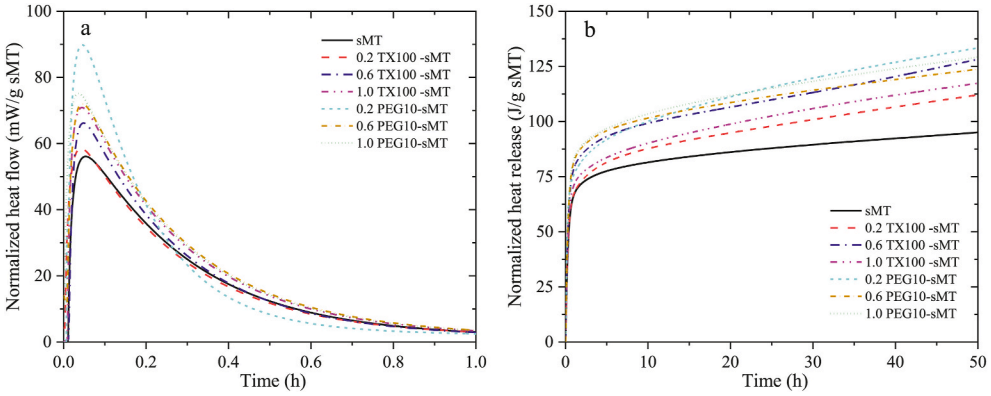

Fig. 17. (a) Normalized specific heat flow and (b) cumulative heat release of the reaction between sMT/OsMTs and CH at 25 °C.

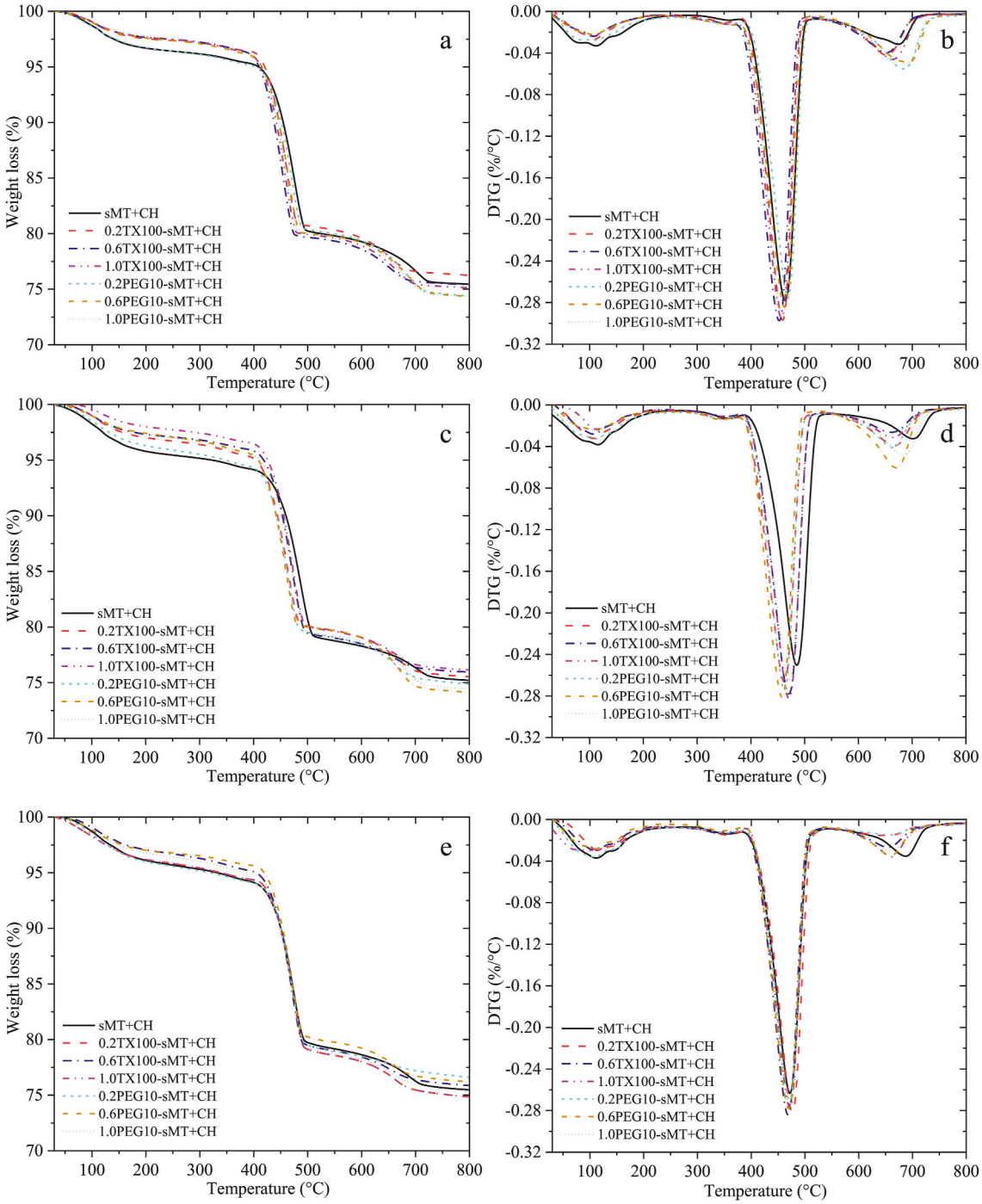

Fig. 18. TGA and DTG curves of binary sMT/OsMT-CH systems at (a, b) 1 day, (c, d) 7 days, and (e, f) 28 days.

exhibit comparable efficiency in enhancing the pozzolanic reactivity of sMT. For TX100 modified sMT, compared with raw sMT, when the concentration of Al + Si was increased to 18.03 mmol/100 g and 28.87 mmol/100 g at 0.6 and 1.0 CEC, respectively, 2.0- and 2.7-times CH consumption were obtained. At the same loadings of PEG10, the increments are 2.2- and 2.6-times, respectively. It was noted that, among the OsMTs, with the highest Al + Si concentrations of 29.46 mmol/100 g and 44.93 mmol/100 g, 0.2TX100-sMT and 0.2PEG10-sMT yielded the lowest CH consumptions of 114.8 g/100 g and 135.8 g/100 g, respectively. This indicates that, in addition to the dissolution of aluminum and silica in the pore solution, other factors, such as particle dispersion, water uptake, and ion absorption, also affect the pozzolanicity and CH consumption efficiency of SCMs.

3.11. Effects on cement composites as an IC agent

The main driving force for applying IC in concrete is to mitigate autogenous shrinkage and self-desiccation cracking. However, it was also reported that the additional pores carried by the traditional IC agents, such as porous super-absorbent polymers and light-weight aggregates, may sacrifice the mechanical strength of cement composites. In contrast to the conventional IC agents, OsMT is fine clay particles with highly pozzolanic reactivity, which normally lead to a more densified microstructure of cement binders [61]. Although this study mainly focuses on the functionalization of sMT and materials characterizations, the early-age autogenous shrinkage (up to 48 h) and compressive strength of the cement composites containing pre-saturated sMT and

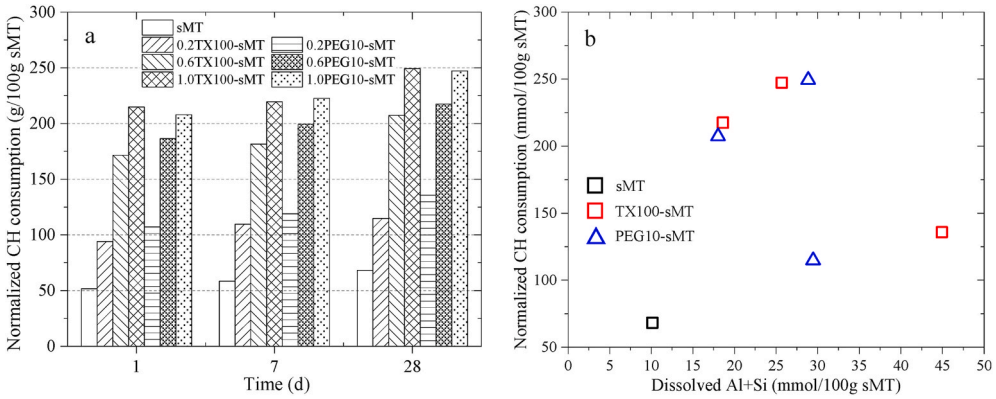

Fig. 19. (a) CH consumption of sMT and OsMTs, (b) the correlations between the released "Al + Si" and the normalized CH consumption.

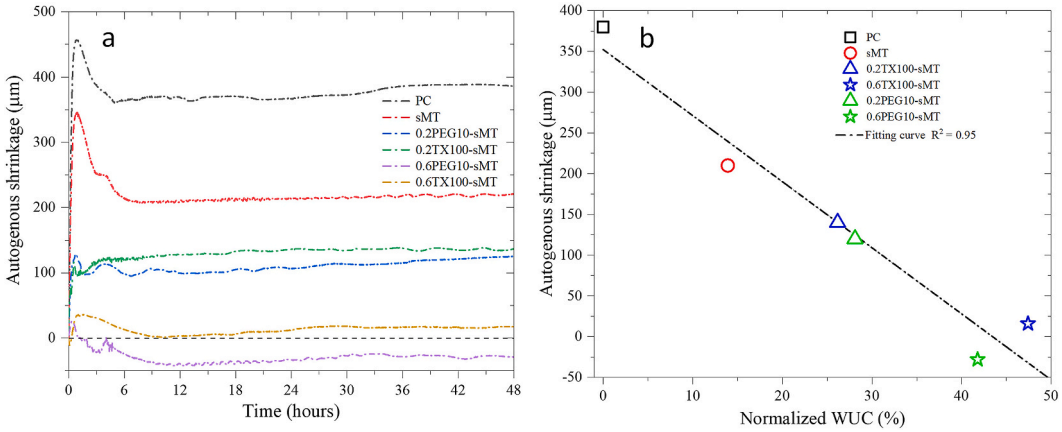

Fig. 20. (a) Autogenous shrinkage of the cement pastes containing 3 wt% pre-saturated sMT and OsMTs, (b) correlation between the normalized WUC of the clay particles and autogenous shrinkage.

OsMTs were investigated to evaluate the feasibility of using the functionalized sMT as an IC agent.

3.11.1. *Autogenous shrinkage*

Fig. 20a illustrates the initial autogenous shrinkage of the cement pastes containing sMT or OsMTs-based IC during the first 48 h. A typical four-stage autogenous shrinkage pattern was captured: stage (i) initial steep sedimentation during the first 1 h, stage (ii) a fall back between 1 and 4 h, stage (iii) a secondary shrinkage after 4 h, and stage (iv) post autogenous shrinkage after 12 h as an equilibrium condition. The initial steep sedimentation stage is a coupled result of the self-compaction with solid fraction moving down under the gravity force and the immediate dissolution of C_3A and its fast hydration reaction once contacting water. The volume expansion (fall back) stage is induced by the crystallization pressure due to the formation of CH and the elevated internal temperature due to cement hydration heat. It can be seen from Fig. 20a that the neat PC displayed the maximum autogenous shrinkage of 456.8 μm at 0.9 h and then stabilized at around 380 μm. The group containing pre-saturated sMT shared the same autogenous shrinkage pattern as the neat PC group but a lower magnitude. The maximum and ultimate shrinkage of the sMT group decreased to 345.6 μm and 210 μm, respectively, which are 24.3% and 44.7% lower than that of the neat PC. In the groups containing pre-saturated OsMTs, the early-age autogenous shrinkage was further reduced. 0.2PEG10-sMT and 0.2TX100-sMT exhibited 67.6% and 64.6% lower shrinkage, respectively, than the PC group. Promising results were observed from the groups with OsMT at 0.60 CEC. 0.6TX100-sMT yielded a 48-h shrinkage of 16.81 μm, which is 95.6% lower than that of the PC group, while in 0.6PEG10-sMT the autogenous shrinkage was eliminated and a slight expansion was observed. This indicates the highly effective role of the OsMTs-based IC in progressively and homogenously moisture releasing outperforming the unfunctionalized sMT. With enhanced pozzolanic reactivity, regulated moisture desorption behavior and better dispersion in the cement matrix, improved cement hydration and a well-densified microstructure can be obtained from the OsMTs-based IC. It was also reported that the autogenous shrinkage decreased with the higher water contents introduced by the IC agents, and the same phenomenon was observed in this study (see Fig. 20b), where a negative linear correlation between the ultimate shrinkage of the cement pastes and the WUC of sMT and OsMT can be observed. These findings reveal the desired effect of decreasing autogenous shrinkage of the cement composites and indicate the effectiveness of the functionalized sMT as an IC agent.

3.11.2. *Compressive strength*

Fig. 21 shows the 28-day compressive strength of the mortars with and without 3 wt% sMT or OsMT. It can be seen that the group containing 3 wt% dry sMT yielded a 7.5% lower strength than the PC group, which might be due to the high-water absorption and agglomeration of sMT particles in the cement matrix. The strength of the group with saturated sMT is 15.5% and 24.8% higher than that of neat PC and Dry sMT, respectively, indicating the benefits of IC in compensating for the side effect of dry sMT on the development of concrete mechanical properties. After functionalization, all the studied OsMT clays-based IC improved the 28-day compressive strength of the mortars. The group of 0.2PEG10-sMT exhibited a compressive strength of 63.4 MPa, which is 20.2% and 5.0% higher than the PC and Sat. sMT groups, respectively. The other OsMT groups (i.e., 0.6PEG10-sMT, 0.2TX100-sMT, and 0.6TX100-sMT) show a comparable 28-day compressive strength, which

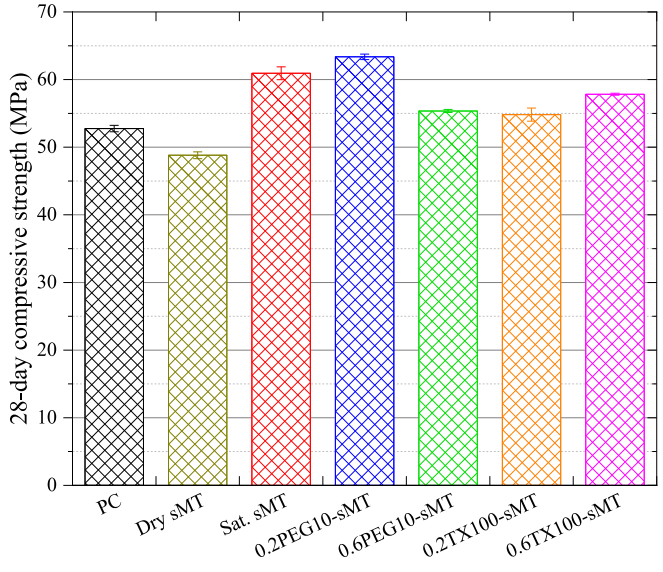

Fig. 21. 28-day compressive strength of mortars with and without sMT/OsMTs-based IC.

is 5.0%, 3.9%, and 9.6% higher than the PC group, respectively, but lower than the groups containing pre-saturated sMT and 0.2PEG10-sMT. The increased mechanical strength might be due to the increased pozzolanic reactivity and better dispersion of OsMT in the cement matrix, as well as the enhanced cement hydration in the presence of IC.

4. Conclusions

The present work investigates the functionalization of sMT with two non-ionic surfactants, TX100 and PEG10, with varying dosages and its influence on the physical and chemical properties of sMT as a potential internal curing agent. Several open research questions were comprehensively addressed: (i) the intercalation of non-ionic surfactants and their influence in altering the interlayer spacing of sMT, (ii) the alteration of dynamic vapor sorption kinetics, water uptake capacity, water release behavior, and hygroscopic swelling behavior, (iii) the improvement of dispersion, ion exchange, and pozzolanic reactivity, and (iv) the effects on autogenous shrinkage and compressive strength of cement composites. The following conclusions can be drawn:

- Both TX100 and PEG10 could be successfully intercalated into the interlayer of sMT and increase the interlayer spacing from 0.56 nm up to 2.31 nm and 2.34 nm, respectively. Compared with TX100, at each dosage, PEG10 exhibits more effective intercalation than TX100. Although interactions between tetrahedral silica sheets with the alkyl chains from surfactants are observed, the bending absorptions of Si–O and Al–O bonds in the aluminosilicate structures of sMT are not significantly impacted by the functionalization.
- With the intercalation of surfactants (both TX100 and PEG10), less time is taken by the OsMTs than the raw sMT to reach equilibrium in both the moisture adsorption and desorption, especially in the RH range between 0 and 30%, resulting in weaker water-clay interaction and a lower moisture vapor absorption. On the other hand, the capillary condensation occurred earlier and was more significant in the OsMTs than sMT, which resulted in a positive correlation between the vapor absorption and surfactant dosage and a comparable final moisture uptake capacity with the raw sMT at 1.0CEC.
- The enlarged interlayer spacing results in reduced hysteresis ("ink-bottle" effect) between adsorption and desorption over the whole RH range in the OsMTs. Different from the moisture absorption, due to the hydrophilic feature of the surfactants and the increased interlayer spacing, the OsMTs yield a significantly increased water uptake capacity.
- The swelling behavior of the OsMT is altered significantly by the organic functionalization, which shows 1.91 to 2.96 times higher than the raw sMT. A positive correlation between the swelling index and water uptake capacity is obtained, which might be favorable to be leveraged as an internal curing agent to reserve extra water to fuel cement hydration and provide tunable space for the deposition of hydration products and deterioration phases, such as ASR gels.
- After functionalization with PEG10 and TX100, the dispersion of sMT in both DI water and simulated cement pore solution is remarkably increased. TX100-sMTs show a higher dispersion than the PEG10-sMTs in both DI water and simulated pore solution under the same surfactant loadings.
- Compared with raw sMT, more Li^+ ions are absorbed and then released by OsMTs, suggesting a more efficient beneficial ion bearing to modify cement hydration and improve concrete durability. The dissolutions of both Al and Si from sMT in pore solution are enhanced by the functionalization.
- Both calorimetry study and lime consumption test show that the pozzolanic reactivity of sMT is significantly increased by the two non-ionic surfactants, which is desirable to further improve cement hydration and concrete properties.
- By incorporating saturated OsMTs, the early-age autogenous shrinkage of the cement composites was effectively suppressed, while a slight increase in compressive strength was obtained, which indicates the high feasibility and efficiency of OsMTs acting as internal curing agents.

This work contributes toward the development of a clay-based dual internal curing to integrate internal curing and pozzolanicity in a single system. The improved physical (moisture absorption, water uptake, tunable swelling, and dispersion), chemical (ion absorption and release, dissolution of Al and Si, and pozzolanic reactivity) properties of the functionalized OsMT with the two non-ionic surfactants, and their effects on properties of cement composites (autogenous shrinkage and compressive strength) provide an evidential indication of leveraging this novel pozzolan in internal-cured concrete. Further complementary investigations remain crucial in elucidating the role of this new internal curing technique in optimizing hydration kinetics and property evolutions of cement composites, which will be the focus of an upcoming study.

Author statement

This manuscript is developed with the following author contributions:

Dayou Luo: Experimentation, Investigation, Validation, Data analysis, Writing- Original draft preparation.

Jianqiang Wei: Conceptualization, Methodology, Data curation, Supervision, Writing- Reviewing and Editing, Funding acquisition.

Declaration of competing interest

The authors declare that they have no known competing financial interests or personal relationships that could have appeared to influence the work reported in this paper.

Data availability

Data will be made available on request.

Acknowledgment

This work was supported by the United States National Science Foundation (NSF) under the CMMI Award (Contract No. 1935799). The

authors gratefully acknowledge the support from this funding.

References

[1] Martino L, Guigo N, van Berkel JG, Sbirrazzuoli N. Influence of organically modified montmorillonite and sepiolite clays on the physical properties of bio-based poly (ethylene 2, 5-furandicarboxylate). Compos B Eng 2017;110:96–105.
[2] Wei J, Gencturk B. Hydration of ternary Portland cement blends containing metakaolin and sodium bentonite. Cement Concr Res 2019;123:105772.
[3] Wei J, Gencturk B, Jain A, Hanifehzadeh M. Mitigating alkali-silica reaction induced concrete degradation through cement substitution by metakaolin and bentonite. Appl Clay Sci 2019;182:105257.
[4] Wei J, Meyer C. Sisal fiber-reinforced cement composite with Portland cement substitution by a combination of metakaolin and nanoclay. J Mater Sci 2014;49 (21):7604–19.
[5] Isaia GC, GASTALDInI ALG, Moraes R. Physical and pozzolanic action of mineral additions on the mechanical strength of high-performance concrete. Cem Concr Compos 2003;25(1):69–76.
[6] Fernández R, Ruiz AI, Cuevas J. Formation of CASH phases from the interaction between concrete or cement and bentonite. Clay Miner 2016;51(2):223–35.
[7] Rahmani H, Asbagh YI. Corrosion resistance of Montmorillonite-modified dense concretes. Int J Civ Eng 2018;16(2):137–46.
[8] Mirza J, Riaz M, Naseer A, Rehman F, Khan A, Ali Q. Pakistani bentonite in mortars and concrete as low cost construction material. Appl Clay Sci 2009;45(4):220–6.
[9] Masood B, Elahi A, Barbhuiya S, Ali B. Mechanical and durability performance of recycled aggregate concrete incorporating low calcium bentonite. Construct Build Mater 2020;237:117760.
[10] Chen M, Liu B, Li L, Cao L, Huang Y, Wang S, et al. Rheological parameters, thixotropy and creep of 3D-printed calcium sulfoaluminate cement composites modified by bentonite. Compos B Eng 2020;186:107821.
[11] Hakamy A, Shaikh F, Low IM. Effect of calcined nanoclay on microstructural and mechanical properties of chemically treated hemp fabric-reinforced cement nanocomposites. Construct Build Mater 2015;95:882–91.
[12] Saravanan S, Ramamurthy PC, Madras G. Effects of temperature and clay content on water absorption characteristics of modified MMT clay/cyclic olefin copolymer nanocomposite films: permeability, dynamic mechanical properties and the encapsulated organic device performance. Compos B Eng 2015;73:1–9.
[13] Uddin F. Clays, nanoclays, and montmorillonite minerals. Metall Mater Trans 2008;39(12):2804–14.
[14] Wyrzykowski M, Ghourchian S, Sinthupinyo S, Chitvoranund N, Chintana T, Lura P. Internal curing of high performance mortars with bottom ash. Cem Concr Compos 2016;71:1–9.
[15] Bentz DP, Snyder KA. Protected paste volume in concrete: extension to internal curing using saturated lightweight fine aggregate. Cement Concr Res 1999;29(11): 1863–7.
[16] Liang G, Liu T, Li H, Wu K. Shrinkage mitigation, strength enhancement and microstructure improvement of alkali-activated slag/fly ash binders by ultrafine waste concrete powder. Compos B Eng 2022;231:109570.
[17] Yang L, Shi C, Wu Z. Mitigation techniques for autogenous shrinkage of ultra-high-performance concrete–A review. Compos B Eng 2019;178:107456.
[18] Powers TC. Physical properties of cement paste. 1960.
[19] Jensen OM, Hansen PF. Water-entrained cement-based materials: I. Principles and theoretical background. Cement Concr Res 2001;31(4):647–54.
[20] Liu L, Fang Z, Huang Z, Wu Y. Solving shrinkage problem of ultra-high-performance concrete by a combined use of expansive agent, super absorbent polymer, and shrinkage-reducing agent. Compos B Eng 2022;230:109503.
[21] Zhutovsky S, Kovler K. Influence of water to cement ratio on the efficiency of internal curing of high-performance concrete. Construct Build Mater 2017;144: 311–6.
[22] Kim H, Lee H-K. Hydration kinetics of high-strength concrete with untreated coal bottom ash for internal curing. Cem Concr Compos 2018;91:67–75.
[23] De la Varga I, Castro J, Bentz D, Weiss J. Application of internal curing for mixtures containing high volumes of fly ash. Cem Concr Compos 2012;34(9):1001–8.
[24] Yang L, Shi C, Liu J, Wu Z. Factors affecting the effectiveness of internal curing: a review. Construct Build Mater 2020:121017.
[25] Cao Y, Wang Y, Zhang Z, Ma Y, Wang H. Recent progress of utilization of activated kaolinitic clay in cementitious construction materials. Compos B Eng 2021;211: 108636.
[26] Muraleedharan MG, Asgar H, Hahn SH, Dasgupta N, Gadikota G, Van Duin AC. Interfacial reactivity and speciation emerging from Na-montmorillonite interactions with water and formic acid at 200° C: insights from reactive molecular dynamics simulations, infrared spectroscopy, and X-ray scattering measurements. ACS Earth Space ChemDev Clay Sci 2021;5(5):1006–19.
[27] Cao Y, Wang Y, Zhang Z, Ma Y, Wang H. Turning sandstone clay into supplementary cementitious material: activation and pozzolanic reactivity evaluation. Compos B Eng 2021;223:109137.
[28] Du J, Min F, Zhang M, Peng C. Study on hydration of illite in K+, Na+, Ca2+, Mg2 +, and Al3+ electrolyte solutions. Z Phys Chem 2019;233(5):721–35.
[29] Kuo W-Y, Huang J-S, Lin C-H. Effects of organo-modified montmorillonite on strengths and permeability of cement mortars. Cement Concr Res 2006;36(5): 886–95.
[30] Yu P, Wang Z, Lai P, Zhang P, Wang J. Evaluation of mechanic damping properties of montmorillonite/organo-modified montmorillonite-reinforced cement paste. Construct Build Mater 2019;203:356–65.
[31] Yang Y, Zhang H, Zeng F, Jia Q, Zhang L, Yu A, et al. A quaternized chitin derivatives, egg white protein and montmorillonite composite sponge with antibacterial and hemostatic effect for promoting wound healing. Compos B Eng 2022;234:109661.
[32] Bergaya F, Lagaly G. General introduction: clays, clay minerals, and clay science. Developments in clay science 2013:1–19. Elsevier.
[33] C837-19 A. Standard test method for methylene blue index of clay. West Conshohocken, PA: ASTM International; 2019.
[34] Taleb K, Pillin I, Grohens Y, Saidi-Besbes S. Gemini surfactant modified clays: effect of surfactant loading and spacer length. Appl Clay Sci 2018;161:48–56.
[35] Jiang Z, Sun Z, Wang P. Internal relative humidity distribution in high-performance cement paste due to moisture diffusion and self-desiccation. Cement Concr Res 2006;36(2):320–5.
[36] Kawamura M, Kasai Y. Methods to determine the saturated surface-dry condition of soils. Geotech High Water Content Mater: ASTM Int 2000;l.
[37] D5890-19 A Standard test method for swell index of clay mineral component of geosynthetic clay liners. West Conshohocken, PA: ASTM International; 2019.
[38] Lothenbach B. Thermodynamic equilibrium calculations in cementitious systems. Mater Struct 2010;43(10):1413–33.
[39] Millard MJ, Kurtis KE. Effects of lithium nitrate admixture on early-age cement hydration. Cement Concr Res 2008;38(4):500–10.
[40] Suraneni P, Weiss J. Examining the pozzolanicity of supplementary cementitious materials using isothermal calorimetry and thermogravimetric analysis. Cem Concr Compos 2017;83:273–8.
[41] Quarcioni VA, Chotoli FF, Coelho ACV, Cincotto MA. Indirect and direct Chapelle's methods for the determination of lime consumption in pozzolanic materials. Rev IBRACON Estruturas Mater 2015;8(1):1–7.
[42] A109/C109M. Standard test method for compressive strength of hydraulic cement mortars (using 2-in. Or [50-mm] cube specimens). 2020.
[43] Kim T, Olek J. Effects of sample preparation and interpretation of thermogravimetric curves on calcium hydroxide in hydrated pastes and mortars. Transport Res Rec 2012;2290(1):10–8.
[44] Zheng L, Jerrams S, Su T, Xu Z, Zhang L, Liu L, et al. Enhanced covalent interface, crosslinked network and gas barrier property of functionalized graphene oxide/ styrene-butadiene rubber composites triggered by thiol-ene click reaction. Compos B Eng 2020;197:108186.
[45] Zhang W, Zou X, Wei F, Wang H, Zhang G, Huang Y, et al. Grafting SiO2 nanoparticles on polyvinyl alcohol fibers to enhance the interfacial bonding strength with cement. Compos B Eng 2019;162:500–7.
[46] Brunauer S, Deming LS, Deming WE, Teller E. On a theory of the van der Waals adsorption of gases. J Am Chem Soc 1940;62(7):1723–32.
[47] Sang G, Liu S, Elsworth D. Water vapor sorption properties of Illinois shales under dynamic water vapor conditions: experimentation and modeling. Water Resour Res 2019;55(8):7212–28.
[48] Joo MH, Park SJ, Hong S-M, Rhee CK, Kim D, Ji G, et al. X-ray micro computed tomography and efficient electrochemical recovery of lanthanides on porous carbon cylinder electrodes. Compos B Eng 2022;231:109590.
[49] Lu N, Khorshidi M. Mechanisms for soil-water retention and hysteresis at high suction range. J Geotech Geoenviron 2015;141(8):04015032.
[50] Guo S, Forooshani PK, Dai Q, Lee BP, Si R, Wang J. Design of pH-responsive SAP polymer for pore solution chemistry regulation and crack sealing in cementitious materials. Compos B Eng 2020;199:108262.
[51] Mitchell JK, Soga K. Fundamentals of soil behavior. New York: John Wiley & Sons; 2005.
[52] Rengasamy P, Sumner M. Processes involved in sodic behavior. Oxford University Press; 1998.
[53] Cao Y, Xu P, Yang W, Zhu X, Dong W, Chen M, et al. UV resistant PBT nanocomposites by reactive compatibilization and selective distribution of tailor-made double-shelled TiO2 nanohybrids. Compos B Eng 2021;205:108510.
[54] Zhang W, Zheng Q, Ashour A, Han B. Self-healing cement concrete composites for resilient infrastructures: a review. Compos B Eng 2020;189:107892.
[55] Pontes J, Santos Silva A, Faria P. Evaluation of pozzolanic reactivity of artificial pozzolans. Mater Sci Forum: Trans Tech Publ; 2013. p. 433–8.
[56] Donatello S, Tyrer M, Cheeseman C. Comparison of test methods to assess pozzolanic activity. Cem Concr Compos 2010;32(2):121–7.
[57] Hakamy A, Shaikh F, Low IM. Characteristics of nanoclay and calcined nanoclay-cement nanocomposites. Compos B Eng 2015;78:174–84.
[58] Junior AN, Ferreira SR, Toledo Filho RD, Fairbairn EdMR, Dweck J. Effect of early age curing carbonation on the mechanical properties and durability of high initial strength Portland cement and lime-pozolan composites reinforced with long sisal fibres. Compos B Eng 2019;163:351–62.
[59] Cao R, Zhang S, Banthia N, Zhang Y, Zhang Z. Interpreting the early-age reaction process of alkali-activated slag by using combined embedded ultrasonic measurement, thermal analysis, XRD, FTIR and SEM. Compos B Eng 2020;186: 107840.
[60] Li Y, Mi T, Liu W, Dong Z, Dong B, Tang L, et al. Chemical and mineralogical characteristics of carbonated and uncarbonated cement pastes subjected to high temperatures. Compos B Eng 2021;216:108861.
[61] Luo D, Wei J. Hydration kinetics and phase evolution of Portland cement composites containing sodium-montmorillonite functionalized with a Non-Ionic surfactant. Construct Build Mater 2022;333:127386.